JGR Earth Surface

RESEARCH ARTICLE
10.1029/2024JF007871

Form and Function of Floodplain Secondary Channels in a Lowland Meandering River System

Tanya Shukla[1] and **Bruce L. Rhoads**[1]

[1]Department of Geography and Geographic Information Science, University of Illinois at Urbana-Champaign, Urbana, IL, USA

Key Points:

- Floodplain secondary channels have muddy banks and beds, are small relative to the main channel, and decrease in size over distance
- Active wood jams are prominent in secondary channels but are more abundant in channels connected to the river at both ends
- Flows exceeding the bankfull stage in the main channel produce nearly full mobilization of cohesive bed material in secondary channels

Correspondence to:

T. Shukla,
tshukla2@illinois.edu

Citation:

Shukla, T., & Rhoads, B. L. (2025). Form and function of floodplain secondary channels in a lowland meandering river system. *Journal of Geophysical Research: Earth Surface*, *130*, e2024JF007871. https://doi.org/10.1029/2024JF007871

Received 10 JUN 2024
Accepted 4 DEC 2024

Author Contributions:

Conceptualization: Bruce L. Rhoads
Formal analysis: Tanya Shukla
Funding acquisition: Bruce L. Rhoads
Resources: Bruce L. Rhoads
Supervision: Bruce L. Rhoads
Visualization: Tanya Shukla
Writing – original draft: Tanya Shukla
Writing – review & editing: Bruce L. Rhoads

Abstract Relatively little is known about the geomorphological characteristics of floodplain secondary channels and the potential for floodplain flows to mobilize bed material within these channels. This study examines the geomorphological characteristics (channel form, material properties, wood jams) and bed-material mobilization potential of secondary channels on the floodplain of a meandering river in Illinois, USA. It also compares these attributes to those of the main channel. Results show that secondary channels are at most about one-third the size of the main channel but also vary in size over distance. Channel dimensions tend to be greatest near the proximal connection of secondary channels to the main channel, suggesting that flow from the main channel is effective in producing scour where it enters secondary channels. The beds of secondary channels consist mainly of mud in contrast to sand and gravel on the bed of the main channel, implying that secondary channels do not convey bed material from the main channel onto the floodplain. Secondary channels connected to the main channel at both ends have more abundant active wood jams than those connected only at the proximal end. Flow from the main channel enters secondary channels at sub-bankfull stages, but maximum mobilization of cohesive bed material in secondary channels only occurs during flows that exceed the average bankfull stage in the main channel. Overall, secondary channels are active conduits of flow, sediment, and large wood on floodplains and can contribute to floodplain sediment fluxes through entrainment of bed material.

Plain Language Summary Floodplains, areas along the main channel of a river that become inundated by water during floods, are carved by channels, referred to here as secondary channels. These channels become submerged as water rises in the river channel. Some of these channels branch off the main channel and then reconnect with it farther downstream. Others originate at the main channel but gradually become indistinguishable as they extend onto the floodplain. In both cases, the channels tend to be the largest where flow enters them from the main channel. Secondary channels contain abundant wood, much of which is transported when water flows through these channels. The beds of secondary channels consist mainly of mud that is mobilized when flow in the main river channel reaches the top of its banks and spills out of the main river channel into the secondary channels. This research supports the emerging perspective that secondary channels are important conduits for conveying water, sediment, and wood from the main river channel on floodplains.

1. Introduction

Floodplains of lowland meandering rivers are often etched with channels activated during infrequent flows that overtop the banks of the main river. These channels, referred to here as secondary channels, are among the first floodplain features to get inundated with rising water levels (David et al., 2017; Lindroth et al., 2020). Secondary channels enhance lateral connectivity between the main river and the floodplain (Czuba et al., 2019; Funk et al., 2023; Lindroth et al., 2020) and can have complex flow dynamics characterized by threshold-dependent flow reversals at certain stages (van der Steeg et al., 2023). From a geomorphic perspective, secondary channels are an important component of the morphological heterogeneity of floodplains (Graf, 2006; Iskin & Wohl, 2023). From an ecological perspective, secondary channels support a variety of ecological functions by serving as habitats (Jones, 2006), contributing to nutrient cycling (Ochs & Shields, 2019) and enhancing biodiversity (Nienhuis et al., 2002; Simons et al., 2001). Because of their morphological and ecological importance, the construction or deepening of secondary channels has become a prominent method of river restoration, particularly in European rivers (Baptist et al., 2004; Buijse et al., 2002; Nienhuis et al., 2002; Schropp & Bakker, 1998; Simons et al., 2001).

The advent of high-resolution topographic information, particularly lidar data, has been a primary factor driving the recognition of floodplain secondary channels as ubiquitous features along lowland meandering rivers (David et al., 2017). Secondary channels are prevalent in river systems across the globe, including tropical (Day et al., 2008; Mertes et al., 1996; Trigg et al., 2012), subtropical (Benke et al., 2000; van der Steeg et al., 2023; Xu et al., 2021), and humid-temperate (David et al., 2017) meandering rivers, as well as in anastomosing arid-zone rivers (Fagan & Nanson, 2004). These channels generally are linear slough-like features, but some meander and have sinuosities as high as 1.6 (Riquier et al., 2015). Secondary channels can occur in isolation and be connected to the main river channel at one or both ends (Cain, 2022) or form networks of interconnected channels (David et al., 2017; Mertes et al., 1996; Trigg et al., 2012; Xu et al., 2020). Although some studies have reported reach-averaged geometrical properties of secondary channels, including width, depth, and width-depth ratio (Fagan & Nanson, 2004; Mertes et al., 1996; Xu et al., 2020), longitudinal variation in the morphology of secondary channels has not been extensively investigated. Also, detailed information on the textural characteristics of the bed and banks of floodplain secondary channels is sparse (Day et al., 2008; Riquier et al., 2015; Sumaiya et al., 2021) compared to the relatively well-documented texture of floodplain-surface deposits (Q. He & Walling, 1998; Moody et al., 1999).

The role of large wood in floodplain dynamics has become a prominent focus of research in river-corridor geomorphic studies (Galia et al., 2024; Lininger et al., 2021; Ruiz-Villanueva et al., 2016; Wohl, 2013), but to date, the amount and spatial distribution of large wood in secondary channels have not been explicitly considered (Latterell et al., 2006). Information on wood in secondary channels is relevant not only for assessing wood dynamics in river corridors but also for modeling sediment transport and floodplain erosion/deposition (Hardy et al., 2000; Marriott, 1992; Nicholas & McLelland, 2004; Nicholas & Walling, 1997; Sumaiya et al., 2021).

Thus, despite increasing recognition of the prevalence of secondary channels on floodplains, few, if any, studies have comprehensively examined the morphologic, sedimentologic, and large-wood characteristics of these channels, particularly in relation to the main river channel. Moreover, the extent to which flows moving through secondary channels during floods can mobilize sediment constituting the boundaries of these channels remains poorly understood. Determining whether floods can mobilize bed material represents a first step toward evaluating whether secondary channels can be eroded by floods, and thus possibly evolve over time, perhaps into anabranching channels (Shukla & Rhoads, 2023). The formation of anabranching channels through enlargement of secondary channels occurs on lowland floodplains prone to channel avulsion (Kleinhans et al., 2012; Makaske et al., 2002, 2017). On the other hand, secondary channels may simply represent depositional sinks for sediment transported into them from the main river during floods and are therefore destined to fill with sediment and eventually disappear. Detailed information on spatial patterns of fluid forces within these channels during floods is needed to better characterize the potential for sediment mobilization and the overall evolutionary trajectory of secondary channels within river-floodplain systems.

The purpose of this research is twofold: to examine the channel dimensions, sediment composition, and large-wood attributes of secondary channels on the floodplain of a lowland meandering river and to determine the extent to which sediment comprising the boundary of secondary channels can be mobilized during floods. A key aspect of the geomorphic characterization and assessment of sediment mobilization is to compare conditions for secondary channels to those for the main river channel. Such a comparison provides the basis for determining how floodplain secondary channels in meandering lowland river systems differ from the main river channel. To accomplish this goal, the research addresses the question: how do the morphology, texture of bed and bank materials, and large-wood characteristics of secondary channels differ from those for the main river channel? A second set of research questions focuses on the erodibility of secondary channels: how do the magnitudes and spatial patterns of bed shear stresses within secondary channels vary as the discharge of the river system varies and what are the implications of changes in the magnitudes and spatial patterns of bed shear stresses for the mobility of bed material within secondary channels? Answers to these research questions provide insight into the distinctive characteristics and process dynamics of floodplain secondary channels, thereby contributing to an improved understanding of the linkages between secondary channels and main river channels in meandering rivers.

2. Study Area

The study area for the research is a ~3 km reach of the Upper Sangamon River (USR) flowing through Allerton Park, an ~8 km^2 tract of land owned by the University of Illinois. The USR flows into Lake Decatur, an artificial

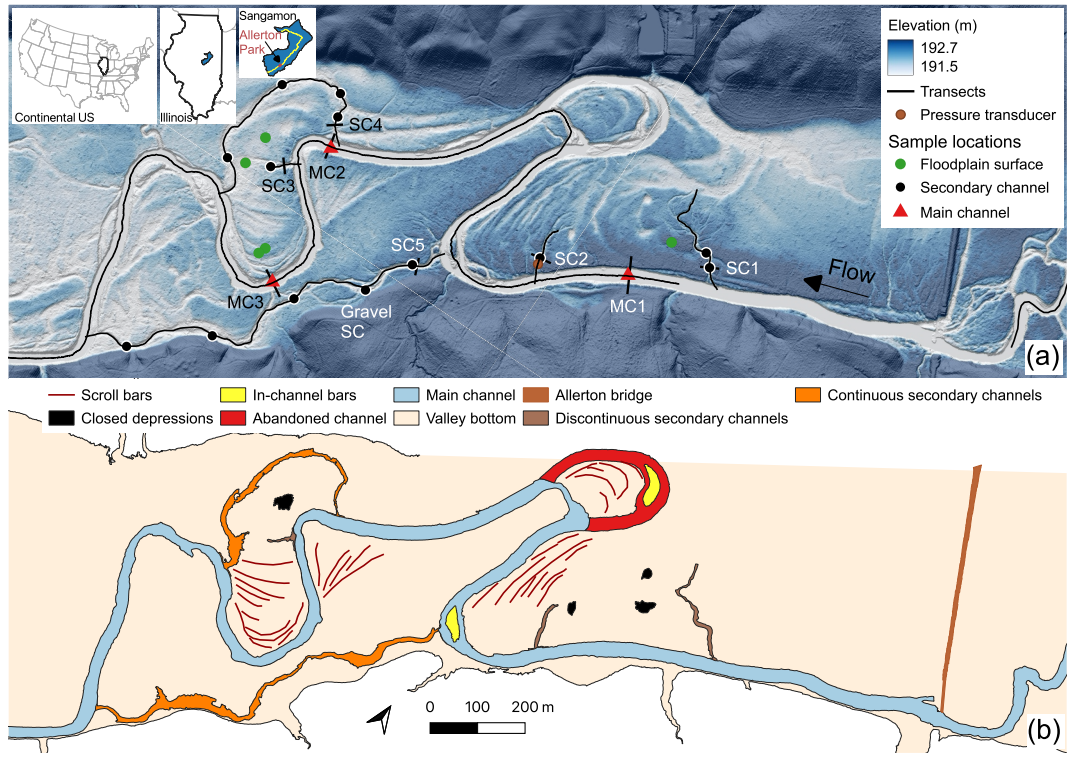

Figure 1. (a) Digital Terrain Model of Allerton Park with location of Allerton bridge, pressure transducer, bed-material sampling locations, and cross-section survey transects. Insets from left to right show the location of Illinois on a map of the continental United States, the location of Sangamon River watershed in the state of Illinois, and the location of Allerton Park in the Sangamon River watershed. (b) A simplified geomorphic map highlighting the prominent floodplain geomorphic features.

reservoir near the city of Decatur, Illinois. Along its ∼174 km length, the river drains an area of 2,400 km^2 of relatively flat agricultural landscape. With an average slope of 1.8%, the USR watershed is characterized by low relief topography sculpted by multiple cycles of advance and retreat of the Laurentide Ice Sheet throughout the Pleistocene Epoch. The most recent ice sheet retreat from the USR occurred ∼17 thousand years ago in the end of the Wisconsin Episode (Curry et al., 2011). Multiple glacial cycles have resulted in 50–150 m of deposits consisting of layers of glacial till, outwash, and lacustrine sediment (Grimley et al., 2016; Kempton et al., 1991). Contemporary soil development in the uplands has occurred in 0.5–1.5 m of loess deposits and underlying glacial sediments (Anders et al., 2018; Fehrenbacher et al., 1986). Current land use within the USR consists of ∼90% cropland, with forests making up less than 3%, largely confined to riparian corridors (Rhoads et al., 2016). Agricultural land use is associated with widespread removal of native vegetation, reworking of the soil through tillage, installation of tile drains, headwater extension of channel systems, and channelization of headwater streams to improve land drainage (Mattingly et al., 1993; Rhoads & Herricks, 1996; Rhoads et al., 2016; Urban & Rhoads, 2003).

The USR watershed is characterized by a humid continental climate regime (Köppen climate classification: Dfa) with cold wet winters and warm dry summers. The mean annual temperature is ∼10°C, with the highest daily average temperatures occurring in July and August (∼25°C) and the lowest daily average temperatures of −5°C occurring during the months of January and February. The mean annual rainfall is 1,000 mm, with spring and fall being the wettest periods (Keefer & Bauer, 2011).

Allerton Park is located about 6 km southwest of Monticello, Illinois. Upstream of Allerton Park, the USR drains an area of ∼1,500 km^2 (Figure 1a). The USR main channel through Allerton Park is about 30 m wide and sits within a 500 m wide floodplain. The average annual discharge of the Sangamon River over the period of record (1908–2023) for a USGS gage at Monticello is ∼12 m^3/s and the largest peak discharge is 390 m^3/s. Bankfull stage at Allerton Park occurs at a discharge of about 42.5 m^3/s (Lindroth et al., 2020). High discharges generally

occur during spring and summer months, while fall and winter are low flow periods. The floodplain at Allerton Park has been minimally disturbed over the last 120 years and is heavily forested with old growth and second old growth forest. The modern floodplain consists of 1.0–1.3 m of silty vertical-accretion deposits overlying 1.2–1.5 m of sandy lateral accretion deposits (Rhoads et al., 2024). Early Holocene alluvium occurs beneath the modern floodplain deposits (Grimley et al., 2017). About 0.8 m of the overbank deposits consists of post-settlement alluvium that has been deposited on the floodplain surface following widespread conversion of land cover in the USR watershed from prairie to intensive agriculture in the mid-1800s (Grimley et al., 2017). Recent work indicates that this transformation of the watershed has not resulted in increased rates of lateral migration of the Sangamon River and that rates of migration remain low (<10 cm/yr on average) (Rhoads et al., 2024). Thus, while the dynamics of the river channel are relatively undisturbed by human activity, impacts of intensive agriculture in the USR watershed cascade downstream and influence floodplain processes.

Five distinct secondary channels have been identified on the Allerton Park floodplain using airborne lidar data collected as part of the Illinois Height Modernization (ILHMP) program covering a centerline length of 1.8 km (Figure 1b). Among the five secondary channels, two (SC4 and SC5) are over 500 m long (550 and 845 m) and are connected to the main channel at both ends (referred to here as continuous secondary channels, CSC). CSCs generally are aligned parallel to the main river valley along the gradient of the floodplain. The other three (SC1, SC2, SC3) are between 80–250 m long, generally originate perpendicular to the main river channel and are connected to the main channel only at one end; the other end of these channels merges with distal portions of the floodplain surface (discontinuous secondary channels, DSC). Of the total river-floodplain area of ∼1 km^2, 10% is occupied by the main channel, and ∼2% by the secondary channels identified in this study. In addition to secondary channels, other prominent geomorphic features on the floodplain include scroll bars and closed depressions (Figure 1b).

3. Data and Methods

3.1. Geomorphic Data

3.1.1. Morphologic Characteristics

Characteristics of bankfull channel morphology of the Sangamon River main channel and floodplain secondary channels were determined using airborne lidar data acquired in 2012 (0.76 m resolution), supplemented by field surveys. These characteristics include bed elevations, bank elevations, channel widths, channel width-depth ratios, and bankfull areas (product of channel width and depth). Morphological characteristics of floodplain secondary channels could be determined from lidar data because the floodplain was completely dry at the time of data acquisition. To evaluate the accuracy of extracting the morphological characteristics of these channels from the lidar data, cross-section elevation surveys of these channels were also conducted in the field in 2022 at several georeferenced locations. Comparison of the ground-survey cross sections with the lidar-extracted cross sections confirmed that cross sections derived from both methods were nearly identical. The elevation surveys were tied to an absolute datum above sea level on a bridge across the Sangamon River at the upstream end of the study reach. For the main channel, bed elevations could not be determined directly from the lidar data because water occupied this channel at the time of data acquisition. To determine bed elevations of the main channel, three georeferenced cross sections of this channel were surveyed in the field at low flow and the elevations of the surveys were tied to the bridge elevation datum. Two of the three cross sections (MC1 and MC3) are located near the upstream and downstream ends of the study reach, with another cross-section within the study reach close to a secondary channel (MC2, Figure 1a).

The workflow to delineate morphology of secondary channels from the lidar consisted of mapping the boundary of the channel feature along contour lines, generating a centerline, creating transects along the centerline, and extracting elevation values along the transects using ArcGIS Pro 2.14. Transects along the centerline were spaced at intervals of approximately one-half of the secondary channel width. Elevation values were sampled across each transect at a spacing equal to the lidar resolution (0.76 m).

The survey data for each transect of the secondary channels were used to determine bankfull geometric properties along the channel centerlines following Lindroth et al. (2020). For a range of water surface elevations from close to the channel bed to above the general floodplain level, the left and right banks were identified, and the corresponding width, depth, area, and width-depth ratio were calculated. When plotted with water surface elevation,

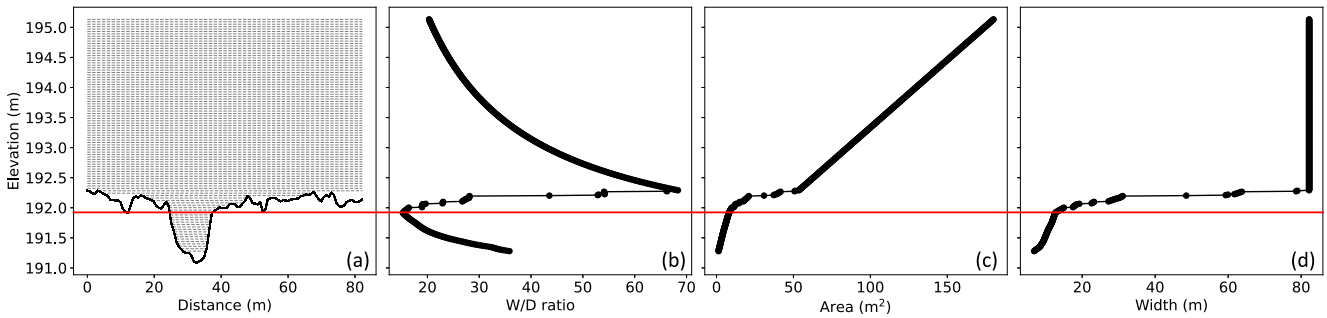

Figure 2. (a) Range of water surface elevations (WSE) tested for a secondary channel transect with associated left and right end points depicted as dashed lines (for clarity, every fifteenth increment of WSE is shown on the graph, (b) variation of WSE with the corresponding values of width-depth ratio, (c) WSE versus inundated cross-section area, and (d) WSE versus cross-section width. The red line depicts the bankfull elevation (192.2 m).

these properties depicted abrupt transitions at the bankfull elevation (Figure 2). These transitions corresponded to the elevation with the lowest width-depth ratio and to breaks in slope in width and area versus elevation.

3.1.2. Textural Characteristics of Channel Bed, Channel Banks, and Floodplain Surface

Bulk samples of sediment were collected from the bed and banks of secondary channels and the main river channel as well as the floodplain surface at various locations throughout the Allerton Park study area (Figure 1). All samples were collected from the top 10 cm of the surface; no armoring or coarsening of the surface bed-material was evident either in the main channel or secondary channels. For the short secondary channel SC3, which had a uniform bed, a sample was collected at one location, whereas for the other secondary channels, samples were collected from 2 to 5 different locations based on visual assessments of spatial variation in texture of the channel bed or banks. Samples for the main channel were collected at the three cross sections surveyed at low flow. Material representing the floodplain surface was obtained from the top parts of cores and auger samples collected in related projects (Grimley et al., 2017; Rhoads et al., 2024).

Overall, a total of 53 sediment samples (39 from the bed and banks of secondary channels, 9 from the bed and banks of the main channel, and 5 from the floodplain surface) were analyzed to determine grain-size distributions. Samples consisting almost entirely (>95%) of sand and gravel were sieved. Samples containing abundant fines (<63 μm) were processed in a Malvern 3000 Mastersizer following appropriate laboratory protocols established by the Illinois State Water Survey. The sediment composition was represented in terms of the percentage of sediment finer than a size class. The percentages of material within three size classes were extracted from the grain-size data, namely: gravel (>2 mm) sand (0.063–2 mm), and mud (<0.063 mm).

3.1.3. Large Wood Characteristics

Accumulations of wood, or wood jams, in the main and secondary channels at Allerton Park were mapped during low-flow conditions to document their properties. Jams included accumulations consisting of at least one large piece of detached wood greater than 2 m in length and 0.2 m in diameter (May & Gresswell, 2003), and jams forming behind live trees. Each jam was photographed and geolocated using a handheld GPS. Various properties of wood jams were documented within secondary channels (Table 1). The diameters and lengths of key pieces were measured with a survey tape and the proportion of the channel width spanned by the jam was determined as the ratio of total channel width to the length of the accumulation. The jam was classified as partial, complete, or active based on its potential to impede flow through the channel and potentially create a hydraulic step (Cashman et al., 2021). Porosity was assessed visually using the recommended field-based procedures (Table 1). The presence/absence of root wads was noted as a proxy of jam movement, and the presence of scour or sediment accumulation associated with the jam was noted to highlight its sediment mobilizing/trapping efficiency. In the main river channel, only the locations of jams were determined because these features were partially submerged in all cases.

Journal of Geophysical Research: Earth Surface

10.1029/2024JF007871

Table 1
Parameters to Quantify Wood Jams Used in This Study

Variable	Unit	Definition	Significance	References
Number of key pieces	NA	The total number of large tree trunks present in the jam	The key pieces stabilize the jam and have the potential to further trap smaller tree branches or leaves	Comiti et al. (2006)
Transport	NA	It was noted whether the jam seems to be comprised of transported material (allochthonous, transported jam) or formed from in-situ material (autochthonous, in situ jam). The primary evidence for in-situ jams is the presence of root wads, leaves, and other branches	Jams comprised of transported wood indicate the general mobility of large wood in the channels	Abbe and Montgomery (2003)
Jam class	NA	Partial—jam only spans part of the channel and consists only of key pieces without any smaller tree material Complete—jam spans >75% of the channel and consists of small tree branches in addition to key pieces, yet is unable to create a step in water level at low flows Active—jam spans >75% of the channel and consists of a combination of key pieces, smaller branches, and leaves, twigs etc. that make the jam sufficiently impermeable to cause a step in water level	The jam class represents the ability of a jam to influence the flow field and, in turn, the channel morphology	Cashman et al. (2021)
Porosity	%	A visual estimate of porosity, made to the nearest 10% estimated by the amount of light that passes through a jam	Porosity is another measure of "void space" in a jam, the presence of smaller tree material tends to block the jam space and leads to less porous jams	Ventres-Pake et al. (2020), Livers et al. (2020), Dixon (2016)
Sediment storage/ Scour pool	Yes/No	Field identification of any morphological changes associated with the jam, including depositional bars, benches upstream/ downstream of a jam or scour pools underneath a jam	The presence/absence of any morphological changes to the channel associated with the jam also point toward its class and porosity, and the impact of changes in hydraulic flow fields across a jam on channel geometry	Abbe and Montgomery (2003), Wohl et al. (2010), Buffington et al. (2002)

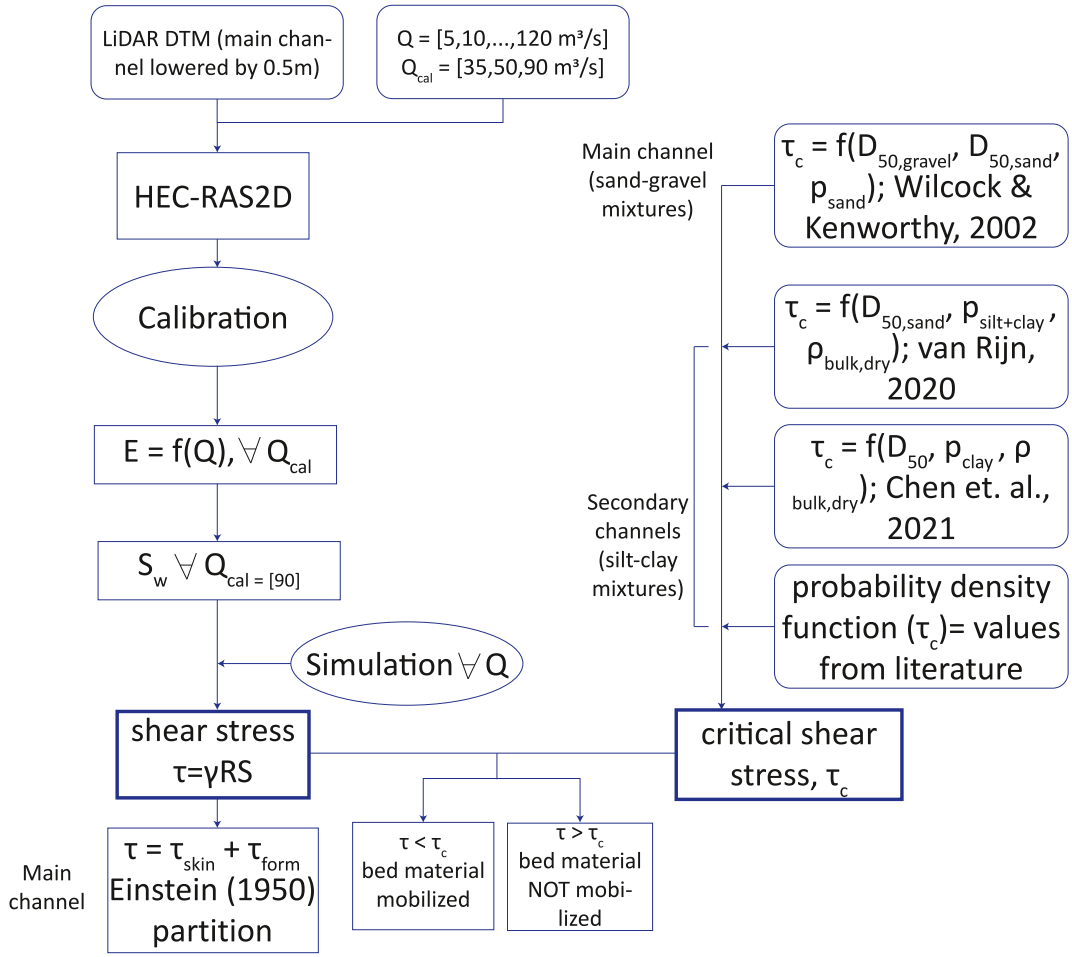

Figure 3. Flowchart for calculation of bed shear stress and critical bed shear stress to determine sediment mobilization potential.

3.2. Spatial Variability in the Potential for Bed-Material Mobilization

The potential for bed-material mobilization within secondary channels and the main river channel was determined by comparing the estimated bed shear stress within these channels for different discharges with the critical shear stress for sediment entrainment (Figure 3). Once entrained from the bed, sediment can be transported as either bedload or suspended load. The goal of the analysis was to evaluate the potential mobility of bed material in secondary channels, particularly in relation to the main channel. Detailed analysis of channel change related to erosion and deposition requires sediment flux calculations, and as such, is beyond the scope of the present work.

Spatial patterns of bed shear stress were estimated based on two-dimensional hydrodynamic modeling over a range of discharges representing different stages of flow within the river-floodplain system. Constant discharges were imposed on the upstream boundary and a normal depth with a friction slope of 0.001 was used as the downstream boundary condition. An existing HEC-RAS2D model of the USR at Allerton Park (Lindroth et al., 2020) was refined by further calibrating the model using additional field data on water-surface elevations during flood events. Three discharges were simulated for calibration: 35 m^3/s, 50 m^3/s, and 90 m^3/s, representing a flow contained entirely within the main channel, a flow confined to the main channel and to secondary channels on the floodplain, and a flow that inundates much of the valley floor, respectively. Calibration involved comparing modeled water-surface elevations with observed water-surface elevations derived from a rating curve at the Allerton Park bridge located approximately 1 km downstream of the upstream model boundary (Lindroth et al., 2020).

Table 2
Results of HEC-RAS2D Calibration

			WSE (m)			Water surface slope		
Q_{sim} (m^3/s)	n_f	n_c	Obs	Sim	DIFF	Obs	Sim	DIFF
35	0.14	0.05	192.22	192.22	0.00			
50	0.1	0.05	192.53	192.52	0.01			
90	0.1	0.04	193.04	193.04	0.00	0.000264	0.000282	1.80E-05

To construct the rating curve, discharges measured using a Sontek M9 Acoustic Doppler Current Profiler were related to absolute elevations of the water surface determined using a water-level sensor tied to a geodetic datum on the bridge. For the 90 m^3/s discharge, the water surface slope (S_w) of the river was also determined from the water-surface elevation at the bridge and the water-surface elevation ~800 m downstream, which was measured using a pressure transducer at the mouth of a secondary channel (Figure 1). The downstream sensor was prone to change in elevation over time but was surveyed only 3 weeks before the 90 m^3/s event. The elevation of the water-surface recorded by this sensor was not considered reliable for the other two discharges because those events occurred many months before or after surveying of the sensor elevation. Calibration involved adjusting values of Manning's friction coefficients for the main channel (n_c) and the floodplain (n_f) in the model until the water surface elevation and, in the case of the 90 m^3/s event, the water-surface slope (S_w) closely matched measured values for the same discharge (Table 2). The calibrated values of Manning's n are similar to those of $n_c = 0.045$ and $n_f = 0.12$ reported by Lindroth et al. (2020) but vary slightly with discharge.

HEC-RAS2D calculates bed shear stresses as $\tau_b = \gamma RS$, where $\gamma =$ the unit weight of water (N/m^3), R is the hydraulic radius (m) calculated as the ratio of wetted area and wetted perimeter for each mesh face, and S is the water surface slope (m/m) between two adjacent cell centers. The model pre-processes the computational domain using the underlying terrain information to generate hydraulic tables for the cells and cell faces and produces mapping of shear stress at the lidar resolution reflecting the sub-grid terrain information (Brunner et al., 2015). The main channel bed consists largely of sand and fine gravel and exhibits no evidence of surface armoring, but can develop bedforms, such as dunes, at high flows. To account for this effect, the bed shear stress τ_b was partitioned into components due to grain friction τ' and form friction τ'' by solving the Keulegan equation for flow depth due to grain friction h' (Garcia, 2008):

$$\frac{U}{\sqrt{gh'S_w}} = 2.5\ln\left(\frac{11h'}{k_s}\right) \tag{1}$$

where S_w is water surface slope, and $k_s = 0.84D_{90}$ is the grain roughness (Wilcock & Kenworthy, 2002). A cross-section average velocity U was obtained from HEC-RAS2D simulations and grain shear stress was calculated as $\tau' = \gamma h' S$. Stress partitioning was not performed for flow in the secondary channels because the beds of these features consist mainly of mud and no reliable methods exist for partitioning shear stresses into grain and form components for this material. Also, existing entrainment relations for mud relate particle erosion to the total bed shear stress.

The critical bed shear stress for sediment mobility within the main channel was calculated using the Wilcock and Kenworthy (2002) subsurface formulation, which explicitly accounts for grain hiding and exposure effects in mixtures of sand-gravel bed material. The sample was separated into sand and gravel fractions and the d_{50} of each fraction (d_g and d_s) was calculated. The critical dimensionless bed shear stresses for the gravel (τ^*_{gc}) and sand fractions (τ^*_{sc}) are given as a function of sand fraction f_s:

$$\tau^*_{gc} = 0.043 - \frac{0.035}{1 + e^{[-25(f_s - 0.16)]}} \tag{2a}$$

$$\tau^*_{sc} = \tau^*_{sc(0)} - \frac{\tau^*_{sc(0)} - 0.045}{1 + e^{[-25(f_s - 0.16)]}} \tag{2b}$$

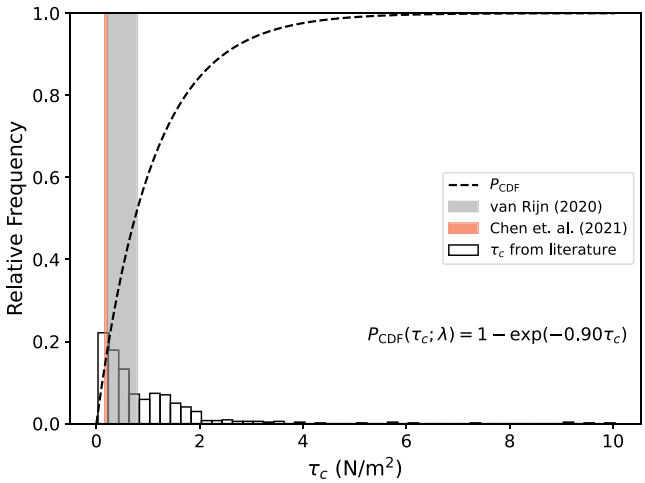

Figure 4. Probability density of τ_c values for erosion of mud from 15 sources, combined with best fit P_{CDF}. Also shown are τ_c from formula by van Rijn (2020) and Chen et al. (2021). Range of τ_c calculated for the secondary channels is shown in shaded colors.

where $\tau^*_{sc(0)} = 0.0774\frac{d_g}{d_s}$. The dimensionless critical bed shear stresses can be converted to dimensional critical bed shear stress for each size fraction d_i

$$\tau_{ic} = \tau^*_{ic}(\rho_s - \rho)gd_i \tag{3}$$

where

$$\tau^*_{ic} = \begin{cases} \tau^*_{sc}, & d_i < 2 \text{ mm} \\ \tau^*_{gc}, & d_i > 2 \text{ mm} \end{cases} \tag{4}$$

and ρ_s is density of sediment (~2,650 kg/m^3), ρ is water density (1,000 kg/m^3), and g is gravity (9.81 m/s^2). Grain mobility of the sediment mixture is determined by comparing the bed shear stress due to grain friction to the critical bed shear stress for each size fraction. Values of shear stress that exceed the critical shear stress are indicative of grain mobility.

Sediment mobility for cross sections within secondary channels was determined by compiling critical bed shear stress values for cohesive mixtures from the literature and calculating a best fit cumulative probability density function (P_{CDF}) (Dunn, 1959; C. He et al., 2021; Hir et al., 2008; Jacobs et al., 2011; Kothyari & Jain, 2008; Panagiotopoulos et al., 1997; Perera et al., 2020; Schäfer Rodrigues Silva et al., 2018; Sharif, 2003; Smerdon & Beasley, 1959; Torfs, 1995; van Rijn, 2020; Zhang & Yu, 2017) (Figure 4). Multiple potential P_{CDF}s were tested: normal, lognormal, exponential, and Weibull. The Kolmogorov-Smirnov (KS) test was used to evaluate the goodness of fit between each P_{CDF} and the critical bed shear stress data set. An exponential function produced the minimum KS statistic measuring the maximum difference between the data and the P_{CDF} (0.056):

$$P_{CDF} = 1 - e^{-0.9\tau_c} \tag{5}$$

The exponential P_{CDF} (Equation 5) was used to calculate the cumulative probability for various values of critical bed shear stress (τ_c). In addition to this probabilistic approach, critical shear stresses were directly estimated based on sediment properties using critical shear stress formulations proposed by van Rijn (2020) and Chen et al. (2021). Both formulations require information on the grain-size distribution and dry bulk density of the sediment mixture —data that were obtained from analysis of samples within secondary channels. The van Rijn (2020) formulation is:

$$\tau_c = \begin{cases} \left(1 + p_{\text{fines}}\right)^{\beta} \tau_{c,\text{sand},0}, & \text{sand fraction} > 63\ \mu\text{m} \\ \left(1 + p_{\text{fines}}\right)^{\beta} \tau_{c,\text{fines},0}, & \text{fine fraction} < 63\ \mu\text{m} \end{cases} \tag{6}$$

where $\tau_{c,\text{sand},0}$ and $\tau_{c,\text{fines},0}$ represent the critical bed shear stresses for erosion of sand and silt fractions. The critical bed shear stresses are based on an empirical fit to experimental data with sediment sizes in the range 10–400 μm (Hoffmans & van Rijn, 2018; van Rijn, 2020):

$$\tau_{c,0} = \frac{0.3}{1 + D_*} + 0.055\left[1 - e^{(-0.02D_*)}\right] \tag{7}$$

with $D_* = d_{50}\left[\frac{g(R-1)}{\nu^2}\right]^{1/3}$, and

$$\beta = \left[1 + \left(p_{\text{clay}}/p_{\text{fines}}\right)^{\alpha 1} + \left(\rho_{\text{dm}}/\rho_{\text{dry,max}}\right)\right]^{\alpha 2} \tag{8}$$

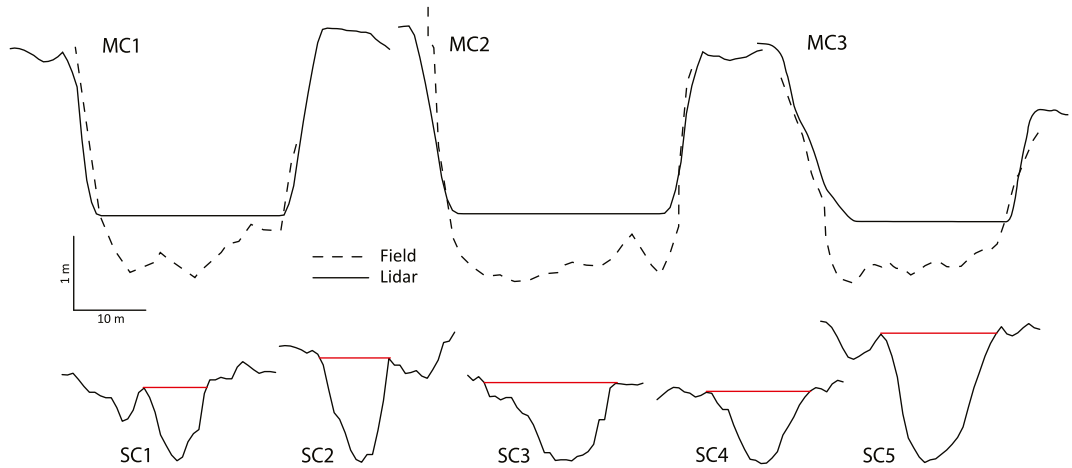

Figure 5. Comparison of cross-section geometry between main-channel cross sections (MC) and secondary-channel cross sections (SC). For the location of cross sections (transects), refer to Figure 1. The red straight line on the secondary channel cross sections depicts bankfull elevation (m) as calculated from the bankfull algorithm used in this study.

Here p_{fines} represents percentage fraction of all sediment <63 μm, p_{clay} denotes percent fraction of sediment <8 μm, ρ_{dm} is the dry bulk density of sediment mixture and $\rho_{\text{dry,max}} \cong 1600\ \text{kg/m}^3$ represents the maximum dry bulk density of mixture. The empirical parameters, as suggested by van Rijn (2020), were defined as $\alpha 1 = 2, \alpha 2 = 1.5$ for the sand fraction and $\alpha 1 = 2, \alpha 2 = 2$ for the fine fraction.

The Chen et al. (2021) formulation is based on a theorical momentum balance analysis under incipient conditions:

$$\tau_c = \begin{cases} \tau_{c,0}\left(\rho_s - \rho\right) g d_s + A \dfrac{1}{d_m}\left(\dfrac{\rho_{dm}}{\rho_m}\right)^{2/3} \times \left[\left(\dfrac{\rho_{dm}}{\rho_m}\right)^{-1/3} - 1\right]^{-2} \times e^{2.4\frac{\rho_{dm}}{\rho_m}}, & p_{\text{clay}} \le p_{\text{clay},c} \\ A \dfrac{1}{d_m}\left(\dfrac{\rho_{dm}}{\rho_m}\right)^{2/3} \times \left[\left(\dfrac{\rho_{dm}}{\rho_m}\right)^{-1/3} - 1\right]^{-2} \times e^{2.4\frac{\rho_{dm}}{\rho_m}}, & p_{\text{clay}} > p_{\text{clay},c} \end{cases} \quad (9)$$

Here, $\tau_{c,0}$ is given by Equation 7, d_s and d_m represent the median grain size of the sand and mud fractions respectively, $p_{\text{clay},c} = 15\%$, and $A = 3.97 \times 10^{-6}\ \text{Jm}^{-2}$ is an empirical coefficient.

The van Rijn (2020) formulation (Equations 6–8) produced critical bed shear stresses between 0.21 and 0.8 Pa, whereas the Chen et al. (2021) formulation (Equation 9) produced a comparatively narrow range of critical bed shear stresses (0.16–0.21 Pa) (Figure 4). The range of critical shear bed stresses resulting from the two formulations correspond to cumulative frequencies ranging from 46% to 93% of the values reported in literature (Figure 4).

4. Results

4.1. Morphology, Sediment Composition, and Wood Jam Characteristics

4.1.1. Morphology

Comparison of cross sections of the main river channel between the field surveys and lidar data shows that flow in the main channel was, on average, about 0.5 m deep at the time of lidar data acquisition (Figure 5). Overall, the main channel is much larger than the secondary channels. The main channel is on average 2.8 times deeper and 2.7 times wider than the secondary channels (Figure 5), but the secondary channels have width-depth ratios only ~0.8 times less than those for the main channel. Thus, although the main channel is much wider and deeper than the secondary channels, the two types of channels have similar width-depth ratios (Figure 5).

Average bankfull properties, particularly width and width-depth ratio, vary among the secondary channels. The two CSCs (SC4, SC5), both of which are over 500 m long, have higher mean widths and standard deviations of

Table 3
Bankfull Properties of Secondary Channels and the Main River Channel

	Average			Standard deviation			
Feature	Depth (m)	Width (m)	Width-depth ratio	Depth (m)	Width (m)	Width-depth ratio	#Transects
Main channel	2.38	34.49	14.47				
Average (Secondary channels)	0.79	12.72	17.54				
SC1	0.76	8.75	13.09	0.40	3.53	5.26	61
SC2	1.03	12.83	13.66	0.33	2.84	4.72	32
SC3	0.68	11.03	18.38	0.33	5.88	8.83	52
SC4	0.58	15.62	29.55	0.21	5.06	11.56	79
SC5	0.88	12.41	16.65	0.43	3.77	8.23	120

width (16 ± 5 and 12 ± 4 m) as well as greater mean width-depth ratios and standard deviations of width-depth ratio (30 ± 12 and 17 ± 8) than the three DSCs that originate at the main channel but dissipate on the floodplain (SC1, SC2, SC3, Table 3). All secondary channels are between 0.6 and 1 m deep, a narrow range compared to that of bankfull width and width-depth ratio.

Longitudinal trends in bed elevations, plotted from the proximal end (i.e., the location where the channel originates by branching off the main channel) to the distal end (i.e., the location where the channel terminates on the floodplain or rejoins the main channel), vary among the secondary channels. All three DSCs (SC1, SC2, SC3) exhibit noticeable increasing trends in bed elevation toward the floodplain interior as they blend with the floodplain surface. This pattern of bed elevation is largely attributable to the occurrence of relatively deep scour pools with low width-depth ratios either close to the proximal ends of the channels (SC1, SC2) or around midway between the proximal and distal ends (SC3) (Figure 6). These three DSCs also cut through prominent levees along the river, producing a decrease in bank elevations toward the distal end of each channel. The increase in bed elevations along with a decrease in bank elevation results in a decrease in channel cross-sectional area, that is, the channels become smaller toward the floodplain interior. By contrast, the two CSCs (SC4 and SC5) exhibit decreasing trends in bed elevation from proximal to distal ends. These secondary channels slope from the upstream location to where the channels rejoin the main channel downstream. The decrease in bed elevation along these CSCs reflects in part the overall decrease in the bed elevation along the floodplain and main channel from upstream to downstream. For SC4, bank-elevation trends mirror bed elevation trends and the channels remain constant in size along their lengths. Pronounced scour produces an exceptionally large deep channel at the proximal end of SC5. Because bank elevations decrease more markedly than bed elevations, the channel cross-sectional area decreases toward the distal end of this channel.

Residuals about trends provide insight into the variability of bed elevations and bank elevations of secondary channels. The RMSE of bed elevation residuals (0.09–0.19) is about 10%–25% of the channel depth, whereas the RMSE of bank-elevation residuals (0.1–0.26) is about 13%–30% of the average bankfull depths. Thus, locally the form of secondary channels as defined by bed elevations, bank elevations, and bankfull area varies substantially along the lengths of these channels.

4.1.2. Sediment Texture

Particle size analysis of bed-material samples shows that the bed of the main channel is composed largely of sand (89%) with some fine gravel (8%), whereas the beds of secondary channels consist mainly of mud (76%) with some sand (24%). For the most part, the median particle size (d_{50}) of bed material in the main channel (d_{50} = 0.35 ± 0.1 mm) is coarser than that in the secondary channels (d_{50} = 0.03 ± 0.1 mm) (Table 4). The high standard deviation of d_{50} for secondary channels is in part due to a site in SC5 that has a d_{50} of 0.2 mm; all other secondary channel bed samples, except one, have median particle sizes between 0.01 and 0.03 mm. A sample from a short reach of SC5, not included in the calculation of mean statistics, has a d_{50} equal to 3.6 mm, an order of magnitude coarser than the median particle size of bed material in the main channel. The source of this exceptionally coarse material is not entirely clear; glacial outwash is typically buried deep (>4 m) beneath Holocene alluvium at Allerton Park and Holocene alluvium analyzed in cores generally is dominated by sand

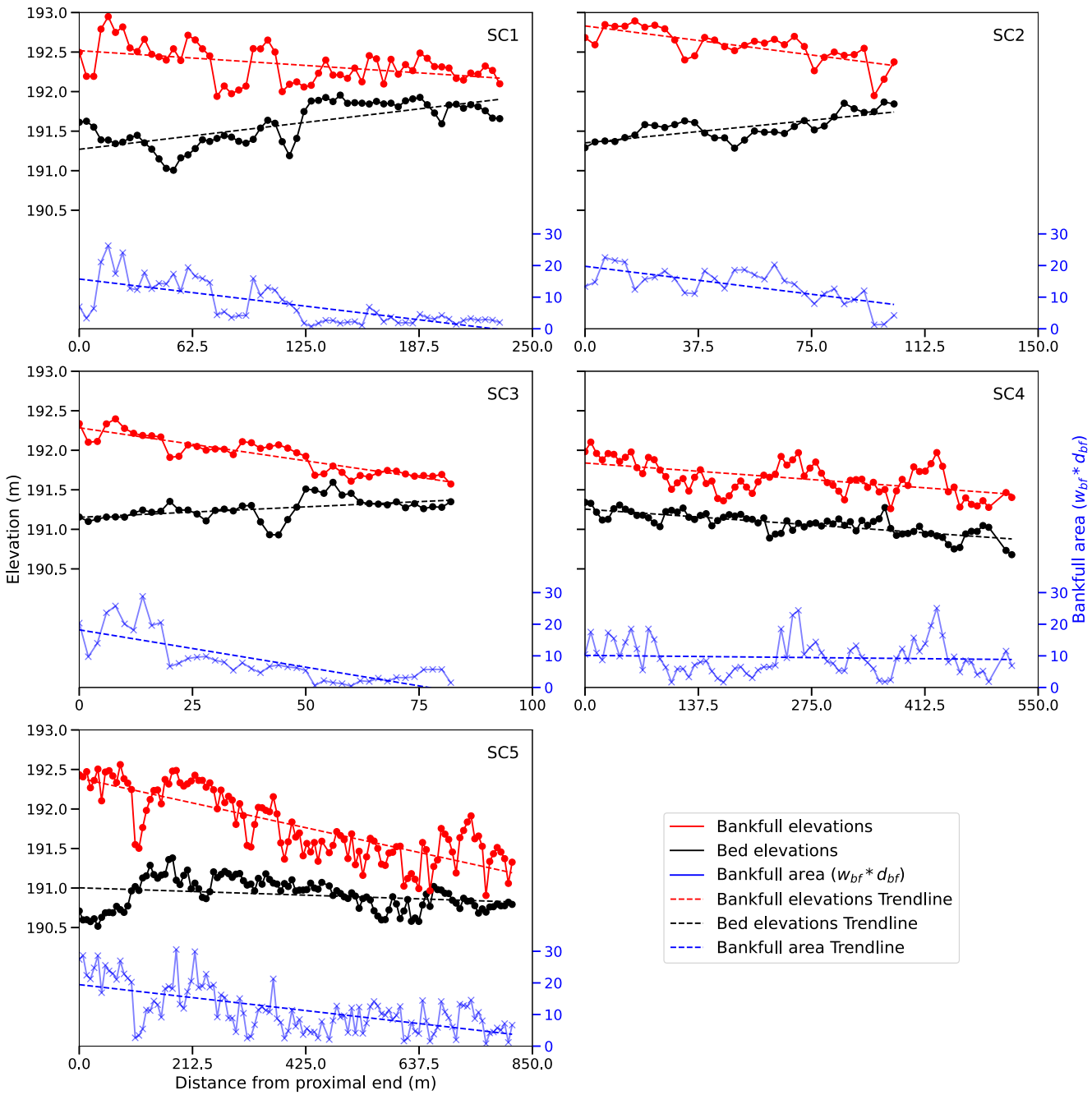

Figure 6. Longitudinal variation in cross-section geometry of secondary channels at Allerton Park floodplain. SC1, SC2, and SC3 represent the discontinuous secondary channels, while SC4 and SC5 are continuous. For locations refer to Figure 1.

(Rhoads et al., 2024). Individual samples (transects) along SC5 have the highest variability of any channel, including the main channel; the sample with d_{50} = 3.6 mm, composed of 59.5% gravel, is located only 120 m away from a sample with d_{50} = 0.007 mm composed of 30% clay.

Although bed material of the main channel and secondary channels differs substantially in texture, bank material of these two types of channels is similar, both in terms of representative grain sizes and fractions of sand and mud (Figure 7). Moreover, average distributions of grain size are nearly identical for bed and bank materials in secondary channels. The median particle sizes of samples of bank material for the main channel and the secondary channels range between 0.01 and 0.03 mm. On average, the texture of sediment on the floodplain surface, which

Table 4
Summary of Sediment Texture Averaging All Samples Belonging to a Geomorphic Feature Class

Feature	Representative grain sizes (mm)		%Fractions		
	d_{50}	d_{90}	Sand	Mud	Gravel
Main channel bed	0.35	1.48	88.9	2.9	8.2
Secondary channel bed	0.03	0.15	23.8	76.2	0.0
Main channel banks	0.02	0.11	19.7	80.3	0.0
Secondary channel banks	0.02	0.11	20.9	79	0.0
Floodplain surface	0.01	0.08	16.0	83.9	0.0
Secondary channel bed SC5	3.63	17.9	37.9	2.6	59.5

consists mainly of overbank deposits (Rhoads et al., 2024) is slightly (≈20%) finer than that of bank material in the secondary and main channels as well as bed material in secondary channels; however, the range of variation in median particle size of floodplain surface material overlaps with the range of variation of bank materials in secondary and main channels as well as bed material in secondary channels.

4.2. Wood Jam Inventory

The wood inventory reveals the presence of abundant wood jams in the main channel and secondary channels. Moreover, the number, distribution, and characteristics of these jams differ in secondary channels versus the main channel. Of the 125 within-channel wood jams in the study area, 85 (68%) occur in the main channel, and 40 are distributed along secondary channels (Figure 8, Table 5). The average spacing of wood jams, expressed as the length of a channel divided by the number of accumulations, ranges from 42 m for SC5 to 68 m for SC1 (Table 5). The average spacing is greater in the three DSCs (SC1–SC3) compared to spacing in the main channel. The average spacing when aggregated over all secondary channels (48 m) is identical to the average spacing of jams in the main channel (48 m). This result reflects the strong influence of abundant wood jams in SC5 on the average of secondary channels. This long secondary channel has more wood jams per unit length than the main channel.

The relative average spacing, the average spacing divided by average channel width, is a scaled metric that accounts for differences in the size of the main channel relative to the size of the secondary channels. Wood jams in the main channel occur at a relative average spacing less than 2 channel widths (Table 5). The relative spacing of wood jams in secondary channels exceeds that of the main channel but is smallest in the CSCs (SC4, SC5) that are connected at both ends to the main channel (Table 5). Relative spacing is greatest for DSCs that terminate on the floodplain (SC1–SC3).

The distance between consecutive wood jams varies from 3 to 189 m for the main channel with a standard deviation of 33 m, or about one channel width. The range of distances between consecutive wood jams in long secondary channels with more than four jams (SC1, SC4, SC5) is less (≈90–125 m) than the range for the main channel (186 m), but standard deviations of spacing are similar (28–38 m) to the standard deviation for the main channel (33 m). When scaled by channel width, the standard deviations for the secondary channels are greater (2–7 channel widths) than the scaled standard deviation of wood spacing for the main channel (1.25 channel width). Average spacing and ranges of spacing do not fully account for clustering of the wood jams, which occur locally in virtually all of the channels. For example, SC2 contains only two wood jams spaced 6 m apart, even though the average spacing of accumulations based on its length is 12 m.

In addition to the spatial location and distribution of wood jams, the field survey reveals key properties of the jams in secondary channels. The majority (60%) of wood jams in all secondary channels have a single key member, are partial wood jams with high porosities of 90%, are not associated with sediment storage or scour, and seem to have been in transport (Figure 9). Fifteen percent of all wood jams are associated with live trees and have no key pieces; all of these types of jams occur in the CSCs that will have water flowing through their entire lengths during flooding. Transported wood jams are clustered in upstream portions of SC1, SC4, and SC5, with most wood jams close to the downstream end of the secondary channels created in situ (Figure 9). Because characteristics of wood jams in the main river channel could not be documented in detail during the survey, comparison of jam properties between secondary channels and the main channel is not possible; however, in general, jams in the main channel, particularly jams spanning a substantial proportion of the channel width, are much larger than those in secondary channels.

4.3. Sediment Mobilization Potential of Bed Material in Secondary Channels

HEC-RAS2D simulations confirm that as stage rises with increasing discharge (Q), secondary channels become activated for discharges less than bankfull flow (≈42.5 m^3/s) (Figure 10). Although shear stresses averaged over the entire secondary channel boundary are initially quite low (0.03–0.7 Pa for $Q = 31.25$ m^3/s), values increase as the floodplain becomes inundated, reaching values of 4–11 Pa for $Q = 120$ m^3/s (Table 6). Among the shorter,

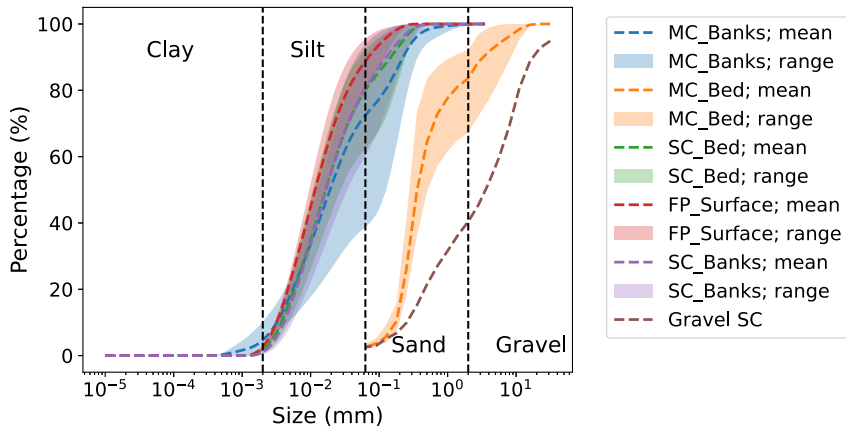

Figure 7. Grain size distribution curves for samples of bed and bank materials for the main and secondary channels and the floodplain surface.

discontinuous secondary channels (SC1, SC2, SC3), the shortest secondary channel SC3 consistently has the highest shear stresses across all discharges (Table 6). The average bed shear stresses within the three DSCs are also higher than those within the two CSCs (SC4, SC5), particularly for discharges exceeding bankfull flow (Table 6). Among SC4 and SC5, the longest secondary channel SC5 has higher average bed shear stresses across all discharges compared to SC4, which has the lowest bed shear stresses of the secondary channels. Thus, while secondary channels are characterized in general by higher bed shear stresses than the rest of the floodplain, considerable variability exists among secondary channels. Moreover, bed shear stresses vary spatially within secondary channels, with the highest bed shear stresses corresponding to regions of pronounced scour that are associated with low width-depth ratios (Figure 10). On the other hand, the average bed shear stress within the main river channel remains within a narrow range of 8–11 Pa, increasing only slightly with discharge.

The bed shear stress typically exceeds the critical bed shear stress for erosion at flows corresponding to bankfull discharge (≈42.5 m^3/s). For secondary channels, the average bed shear stress at the sampled transects equals the 90% cumulative probability of exceeding the critical bed shear stress for flows between 40 and 60 m^3/s (Figure 11b). Although in a few cases (transects 3A, 4B, 4D, 5B, 5D) the bed shear stress decreases somewhat for large valley-filling flows (70–120 m^3/s), the probability of bed-material mobilization remains high (≈80%) for

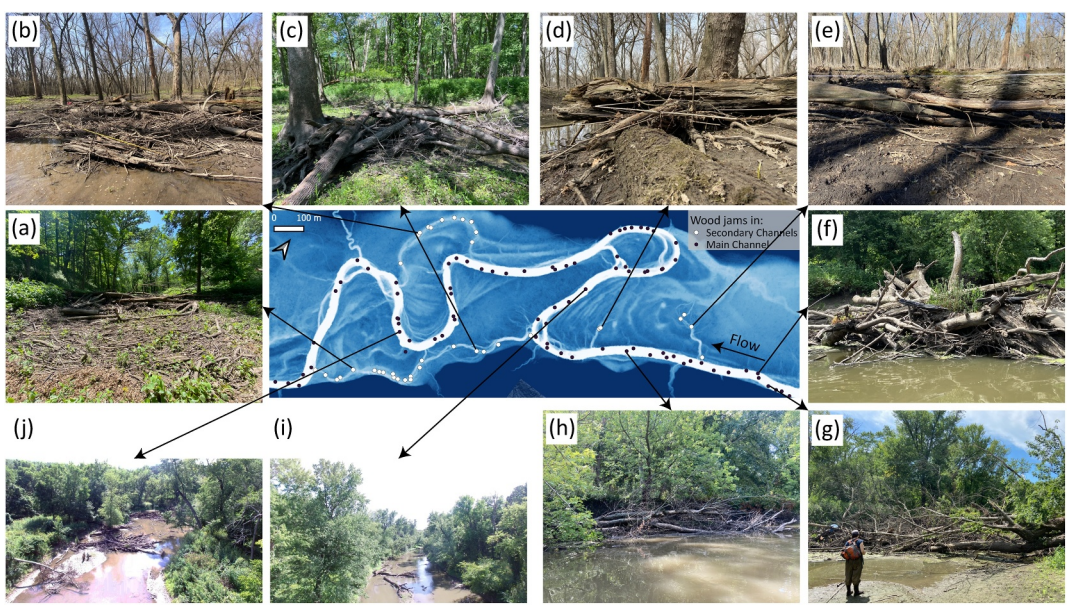

Figure 8. (a)–(e): Wood jams in the secondary channels; (f)–(j): wood jams in the main river channel.

Table 5
Wood Jams in Secondary Channels

Feature	Length (m)	Avg. Width (m)	# of wood jams	Length/ #jams (m)	Length/ #jams/width	Range of consecutive spacing (m)	Standard deviation of consecutive jam spacing (m)	Standard deviation of consecutive jam spacing/width
MC	4,049	26.0	85	48	1.8	186	33	1.25
SC1	270	5.5	4	68	12.2	91	38	6.88
SC2	131	5.6	2	66	11.7	6	6	1.11
SC3	89	5.8	0	0	0	0	0	0.00
SC4	579	10.6	12	48	4.5	124	38	3.61
SC5	882	12.9	21	42	3.3	111	28	2.18
Total SC	1,934	10.4	40	48	4.7	66	22	2.13

these flows (Figure 11). For the two main channel transects (MC1 and MC2), the discharge that mobilizes all bed material is between 27.5–42.5 m^3/s (Figure 11c). In the case of the single secondary-channel transect where bed-material also consists of sand and gravel (SC 5E, Figure 11a), the discharge corresponding to a 90% probability of bed-material mobility is 60 m^3/s—slightly above bankfull flow when water spills into this secondary channel from the main channel. At lower discharges, only sand to fine gravel material has critical shear stresses that exceed the shear stress (Figure 11c).

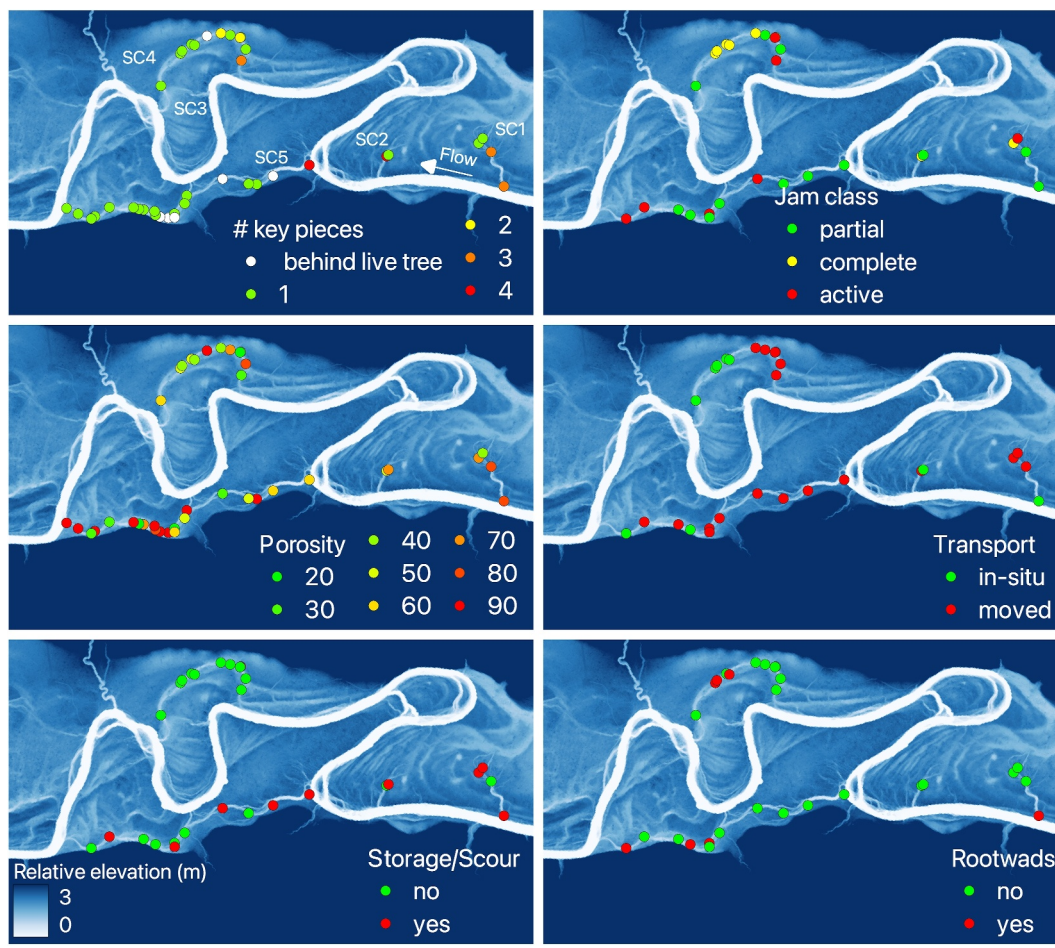

Figure 9. Wood jams in secondary channels classified based on jam parameters.

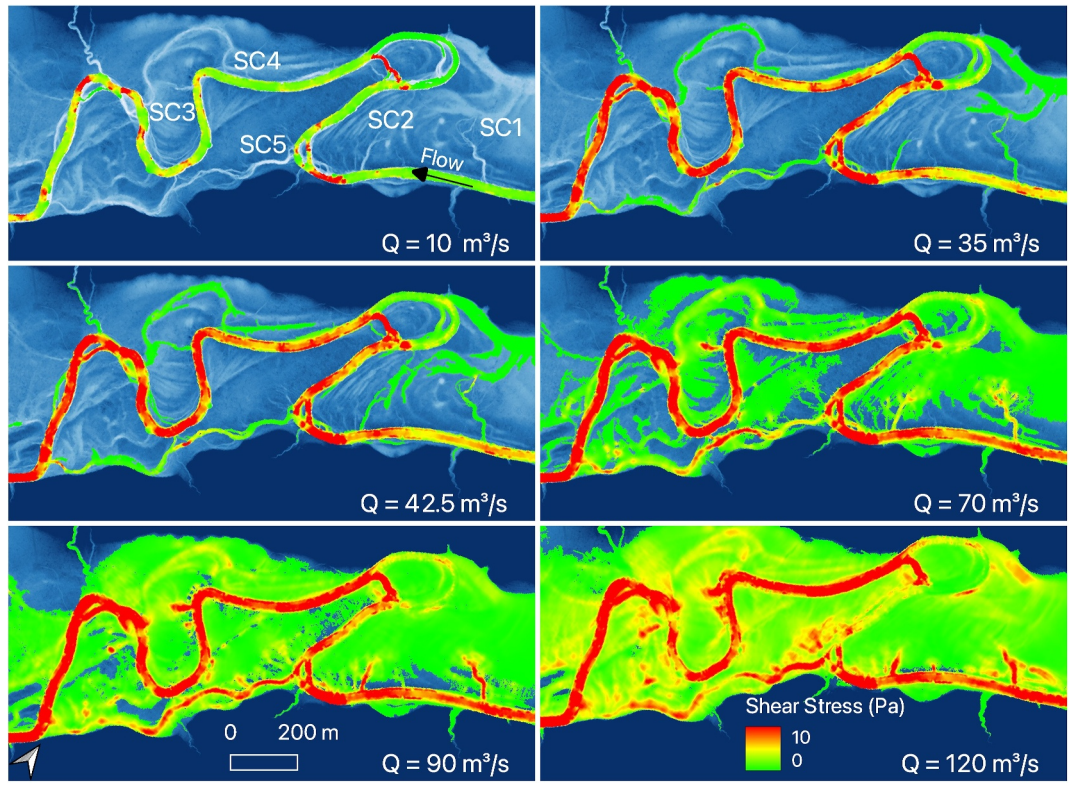

Figure 10. Shear stress distributions for simulated flows.

5. Discussion

The findings of this study support the following answers to the two research questions posed in the introduction. The secondary channels at Allerton Park are ~3 times smaller in width and depth than the main river channel (Table 3, Figure 5), consist of sediment similar to the bank material of the main channel but slightly coarser than the floodplain surface (Table 4, Figure 7), and contain abundant wood jams (Table 5), similar to the main river channel. Moreover, while secondary channels become inundated at flows below bankfull stage, the probability that bed shear stresses in these channels exceeds the critical bed shear stress of cohesive mixtures remains relatively low (0%–50%) for sub-bankfull flows but increases to ~90%–100% after the bankfull discharge is exceeded (Figure 11). The probability of bed-material movement in secondary channels approaches 100% for floods large enough to inundate most of the valley bottom. Thus, the bed material within these channels, although fine-grained

Table 6
Bed Shear Stress Values Averaged Over Secondary Channel Boundary

	τ_b (mean ± std dev) over the entire secondary channel polygon feature (N/m^2)					
Discharge (m^3/s)	MC	SC1	SC2	SC3	SC4	SC5
31.25	8.02 ± 5.41	0.03 ± 0.21	0.12 ± 0.54	0.35 ± 0.80	0.06 ± 0.41	0.71 ± 0.82
35	8.67 ± 5.70	0.35 ± 0.68	0.12 ± 0.55	0.40 ± 0.95	0.20 ± 0.54	1.31 ± 1.40
42.5	8.99 ± 5.33	0.98 ± 1.45	0.12 ± 0.54	0.53 ± 0.88	0.71 ± 0.59	1.99 ± 1.94
50	9.01 ± 4.78	1.57 ± 1.82	0.19 ± 0.52	2.06 ± 1.85	1.21 ± 0.62	2.59 ± 2.46
60	9.88 ± 5.18	3.18 ± 1.41	1.36 ± 0.61	4.93 ± 2.83	2.14 ± 0.85	3.75 ± 2.71
70	10.44 ± 5.44	5.08 ± 1.32	4.22 ± 0.62	7.34 ± 2.52	2.94 ± 1.07	5.02 ± 2.66
90	11.00 ± 5.82	7.65 ± 3.83	8.36 ± 2.08	10.41 ± 3.58	3.76 ± 1.35	6.66 ± 2.59
120	10.94 ± 5.59	7.66 ± 4.29	8.79 ± 4.42	11.30 ± 4.81	4.21 ± 1.59	7.78 ± 3.56

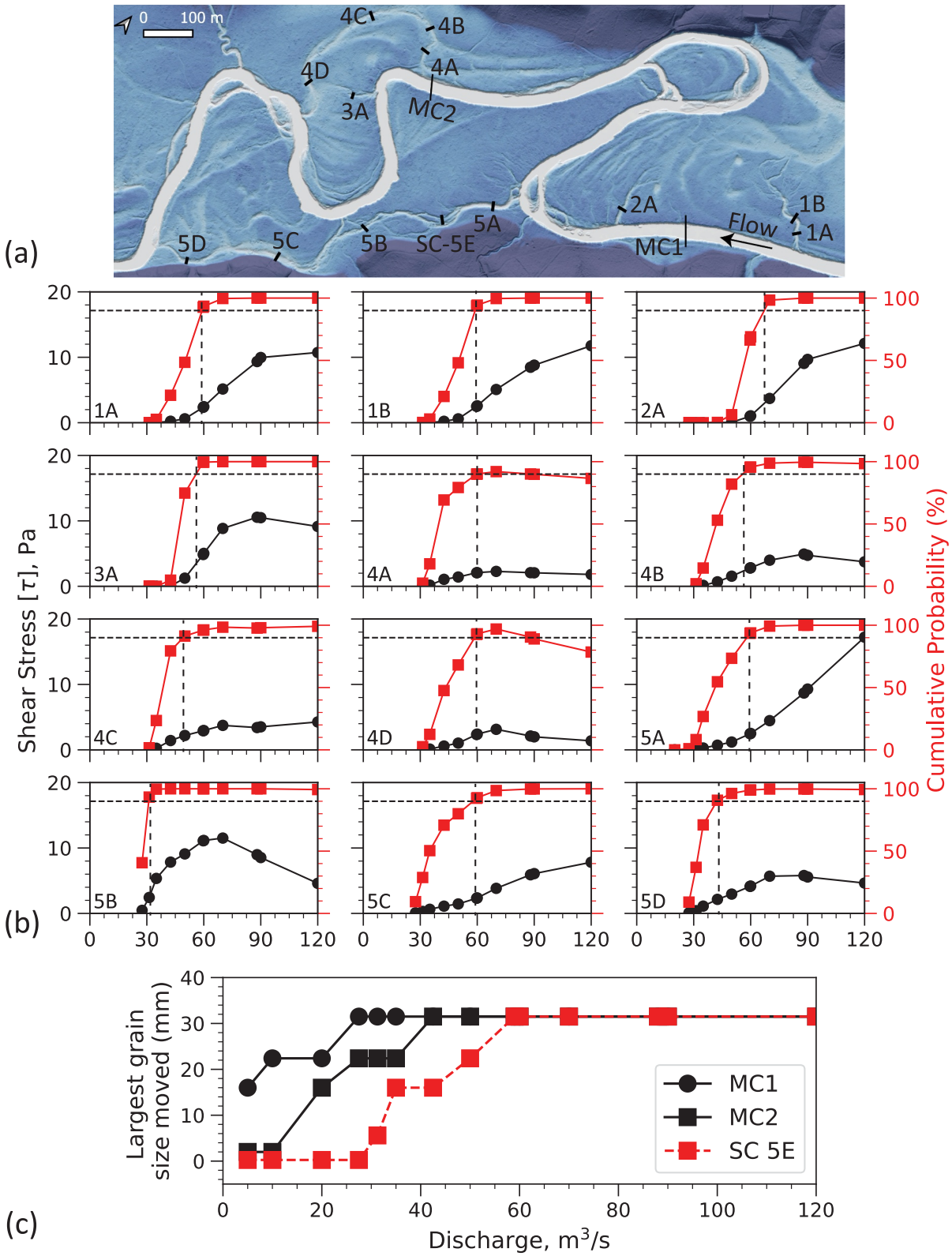

Figure 11. (a) Map of Allerton Park floodplain depicting transect locations where sediment sampling was undertaken. (b) Variability of bed shear stress with discharge at the transects. Secondary *y*-axis depicts the probability of sediment mobilization based on the best fit exponential CDF of critical bed shear stress for silt-clay mixtures (see Figure 4). The dotted black horizontal line on all plots represents 90% probability of sediment movement and the corresponding discharge is shown by the dotted vertical line. (c) Grain mobility variation with discharge for the three transects with non-cohesive sediment.

and cohesive, is capable of being readily mobilized during flood events that exceed the capacity of the main channel.

Comparison of the characteristics of the secondary channels examined in this study with those documented elsewhere is constrained by limited information on these types of channels. Floodplain secondary channels along the East Fork White River (EFWR) in Indiana are about as wide as the main channel but half as deep, resulting in a width-depth ratio of the main channel that is only 0.4 times that of the secondary channels. Grain size data are not reported for the EFWR main-channel bed, but bed material in secondary channels consists mainly of fine sand ($d_{50} = 0.4$ mm) rather than mud (Sumaiya et al., 2021). Moreover, secondary channels along the EFWR occur as dense networks, compared to the channels at Allerton Park, which are isolated features that do not intersect one another. The reason for these differences in secondary-channel characteristics for two nearby midwestern rivers is not entirely clear, but may reflect higher fluvial energy of the EFWR as indicated by the sandy characteristics of its bed material and floodplain surface sediment ($d_{50} = 0.4$ mm).

5.1. A Continuum Within a Continuum: Spatially Variable Secondary Channel Morphology Influences River-Floodplain Connectivity

An important geomorphic characteristic of secondary channels revealed in this study is the spatial variability in bankfull geometry (Figure 6). Spatial variability in bankfull elevations of secondary channels implies a continuum of floodplain inundation as water rises and spills onto the floodplain surface non-uniformly along the length of these channels. Through this process, low-lying portions of the floodplain surface become interconnected by flow through a network of negative-relief features that evolves continuously with increases in stage. Such networks of floodplain flow paths also occur on river floodplains elsewhere, indicating that spatial and temporal variability in floodplain inundation is driven by spatial variability in floodplain topography (Castillo et al., 2020; Czuba et al., 2019; Lindroth et al., 2020; Sumaiya et al., 2024; Trigg et al., 2012; Xu et al., 2020). Previous work on the USR at Allerton Park has shown that spatial variability in bankfull elevations for the main river channel primarily reflects spatial variability in channel planform and the locations of secondary channels (Lindroth et al., 2020). This work has contributed to the emerging paradigm in which floodplain inundation is viewed as occurring not abruptly at a distinct bankfull stage but gradually over a range of stages associated with the complex geomorphology of the river-floodplain interface (Czuba et al., 2019; Lindroth et al., 2020; Xu et al., 2021). At Allerton Park, the largest deviations from a linear bankfull elevation trendline correspond either to differences in bank elevations for the inner and outer banks at meander bends or to local lows in the channel banks where secondary channels branch from or rejoin the main channel (Lindroth et al., 2020). Locally, main-channel bank heights where secondary channels connect with the main channel can be 50%–75% less than nearby bank heights even though the bed of the main channel is 1–1.5 m lower than the entrance to secondary channels. The RMSE of residuals of bank elevations for the main channel about a general trend line is about 10% of the bankfull depth for the main channel (Lindroth et al., 2020). By contrast, the RMSE of deviations in bankfull elevations of secondary channels is between 13% and 30% of the bankfull depth. Thus, these channels have more variable bankfull elevations than the main channel.

Local lows in secondary-channel bank elevations often occur where these channels intersect linear sloughs or other negative relief features, whereas local highs develop where secondary channels traverse positive relief features such as levees or scroll bars. On the floodplain surface, secondary channels act as key regulators of surface-water connectivity between these channels and the rest of the floodplain surface. In other words, similar to the main channel, bankfull elevations of secondary channels are associated with spatial variability in the elevation of the adjacent floodplain topography so that overtopping of secondary channels occurs over a range of water-surface elevations. The irregularity of bankfull elevations along secondary channels allows water to spill readily into surrounding sloughs, even for flows that do not widely inundate the floodplain surface. Hydrodynamic modeling of inundation in the Allerton Park reveals an interconnected network of topographic lows, or poorly defined sloughs, that connect flow in all five secondary channels studied here to flow in the main channel at bankfull stage (Figure 10).

The directionality of transport-effective flows within secondary channels is yet to be conclusively determined. Recent modeling work predicts that water generally moves toward the floodplain from the main channel on rising limbs of floods but can drain back toward the main channel during falling limbs (van der Steeg et al., 2023). On the other hand, field observations indicate that draining of water back into the main channel through levee breaches is fairly rare and that water generally flows toward the floodplain from the main channel throughout

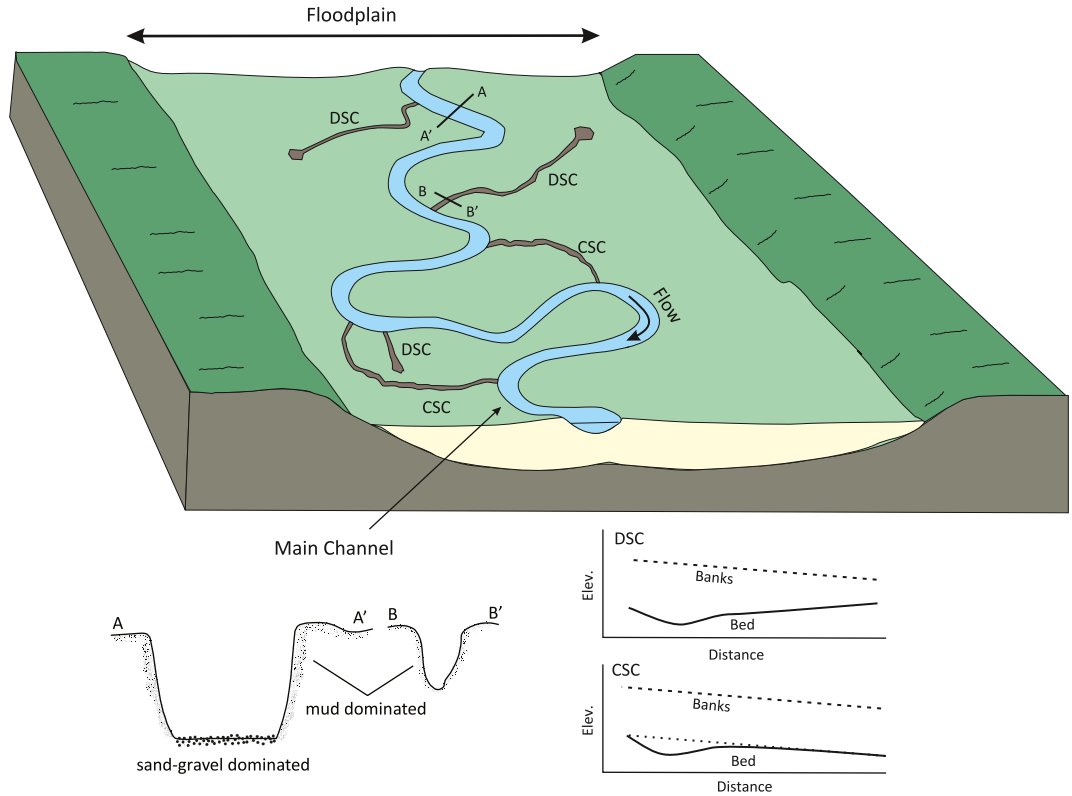

Figure 12. Conceptual diagram of floodplain secondary channels on a lowland meandering river showing discontinuous (DSC) and continuous (CSC) types of channels, different in cross-sectional shape and material properties, and elevation profiles of the channel bed and channel banks of DSCs and CSCs (dotted line represents bed profile of CSC without scour).

floods (Tull et al., 2024). The simulations in this study, which are conducted for steady conditions, show that flow is generally directed through the secondary channels from the proximal to distal ends. Further work is needed to document flow within secondary channels in the field to determine how water moves through these channels during floods.

5.2. Implications for Bed-Material Transport Connectivity

Aside from surface-water connectivity, an order of magnitude difference in bed-material texture between the main channel and secondary channels suggests that bed-material transport in the main channel is largely disconnected from sediment transport in the secondary channels. Flows entering the secondary channels seem to transport predominantly wash load and fine suspended load (Salas & Rhoads, 2024). The main factor influencing this disconnectivity is the discordance between the elevation of the main-channel bed and the elevation of the secondary channel bed at its proximal end. In discordant secondary channels, coherent secondary circulation may drive exchange of suspended sediment between the main channel and a lateral channel (Chowdhury et al., 2022; Herrero et al., 2015). Further analysis is needed to determine whether secondary channel bed material is derived from eroded floodplain deposits or from suspended load from the main channel that is deposited within these channels.

5.3. A Conceptual Model of Secondary Channels on Muddy Meandering-River Floodplains

The floodplain geomorphology at Allerton Park provides the basis for a provisional conceptual model of secondary channels on muddy meandering-river floodplains based on differences in morphological connectivity with the main channel. This model includes DSCs that are connected to the main channel at only one end and CSCs that are connected to the main channel at both ends (Figure 12). DSCs generally are widest and deepest close to the main channel where river flow enters the secondary channel, while away from the main channel, the beds of DSCs merge with poorly defined sloughs and the floodplain surface, at which point they become indistinct.

Discontinuous secondary channels have been identified on floodplains elsewhere and have bed profiles similar to DSCs at Allerton park (Benke et al., 2000; Rowland et al., 2009; Thayer & Ashmore, 2016). Similar to DSCs, CSCs also tend to have large, well-defined cross sections near their proximal ends. In contrast to DSCs, these channels do not become indistinct over distance, but maintain comparatively small, yet well-defined cross sections toward their distal ends. Bank and bed profiles of CSCs may or may not be parallel depending on the extent to which scour occurs near the proximal ends of these channels (Figure 12).

5.4. How Do Secondary Channels Form and Evolve?

The origin and evolutionary trajectory of secondary channels at Allerton Park remains uncertain given the lack of long-term information on the development and change in these features. The negative relief of secondary channels in relation to the elevation of the floodplain surface implies an erosional origin, possibly through reactivation of pre-existing topographic lows on the floodplain (David et al., 2017, 2018). The results of the HEC-RAS2D simulations support the inference that flow through these channels mobilize and rework bed material. Four of the five secondary channels (all three DSCs—SC1, SC2, SC3 and one CSC–SC5) have the largest cross-sectional areas at or close to their proximal ends, suggesting that scour has occurred close to the connection with the main channel. Pronounced scour about mid-distance along SC3, the shortest discontinuous secondary channel, resembles erosion within downstream elongating embayments that develop in early stages of some chute cutoffs (Constantine et al., 2010; Thompson, 2003; Viero et al., 2018). The location of SC3 close to the apex of a meander bend with high curvature suggests this feature may either be a chute channel in development or a failed chute cutoff (van Dijk et al., 2014). The length and curved planform of SC4, the second longest secondary channel, indicates that it may be an abandoned meander bend that is gradually filling in through sedimentation. Whether or not gradual infilling would maintain roughly parallel profiles of bankfull and bed elevations as is the case for SC4 is uncertain; in many cases infilling of cutoff bends occurs unequally throughout the length of the bend (Constantine et al., 2010), but some cutoff infills do exhibit systematic decreases in elevation over distance (Piégay et al., 2008) Also, the HEC-RAS2D modeling indicates that the bed of this feature is mobile during floods and the occurrence of numerous wood jams suggests that active transport of wood is occurring through this channel.

The analysis of bed-material mobilization potential supports the notion that secondary channels at Allerton Park are morphodynamically active. Bankfull discharge, which occurs on average 30 days per year at Allerton Park, tends to be the threshold flow that activates the general mobilization of sand and mud in secondary channels. Additionally, discrete deposits of medium to coarse sand have been observed within secondary channels (Figure 13d), indicating that flows in these channels are locally competent to transport relatively coarse material either in suspension or as bedload—a finding consistent with recent modeling of sediment transport in floodplain channels elsewhere in the US Midwest (Sumaiya et al., 2021). This conclusion is also supported by pronounced zones of scour, vertical cutbanks, and exposed root systems at some locations within secondary channels (Figures 13e and 13f). Thus, field evidence suggests that both erosion and deposition occur in secondary channels. Erosion is likely to be active at above-bankfull flows in the main channel when the beds of secondary channels are mobile (Sumaiya et al., 2021), whereas deposition is likely to occur at sub-bankfull flows in the main channel when flows in secondary channels cannot readily mobilize bed material and local ponding of water after floods promotes net deposition of fine suspended sediment. SC4, the long winding secondary channel on the northwestern region of Allerton Park generally has the lowest shear stresses of any of the secondary channels; these low stresses are consistent with the inference that this channel may be a meander scar that is infilling over time.

The persistence of secondary channels at Allerton Park is difficult to ascertain from historical aerial imagery, most of which has been obtained during summer leaf-on conditions that obscure these channels. Available evidence on channel migration of the main channel (Rhoads et al., 2016, 2024), the evolution of cutoffs along the main channel (Figures 13a and 13b), and short-term observations of the effects of floods on secondary-channel morphology over the span of a few years all suggest that the morphodynamics of the main channel and secondary channels in this lowland meandering river are protracted, with changes in morphology occurring over decadal timescales, rather than at the scale of individual flood events. The availability of repeat aerial lidar data of the floodplain of the river in the future should provide an opportunity to evaluate the morphological evolution of these channels over decadal timescales.

The occurrence of distinct secondary channels on the Sangamon River floodplain raises the question of whether these features can evolve into anabranching channels. In contrast to secondary channels, anabranching channels

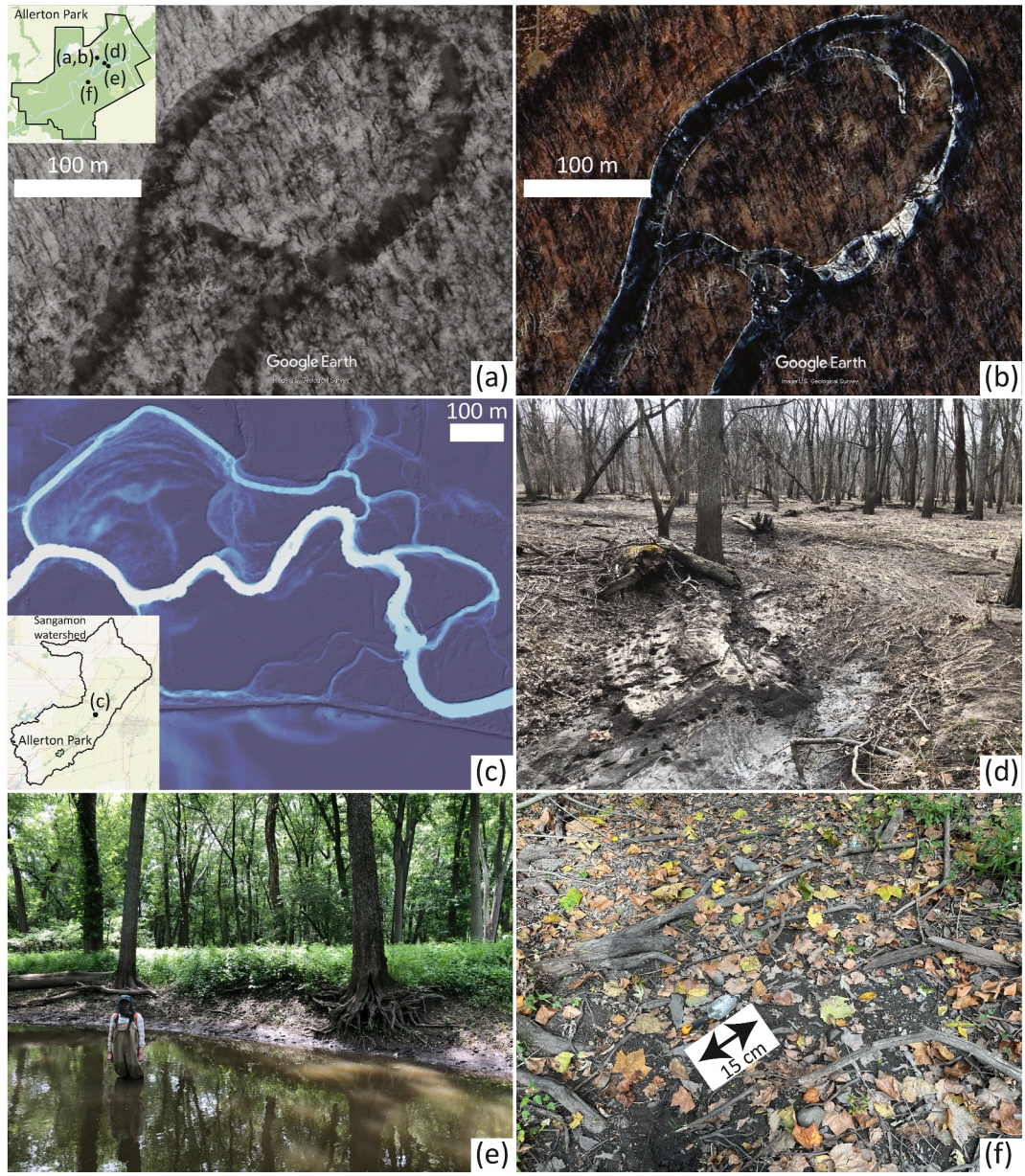

Figure 13. (a) Cutoff of a meander loop along the Sangamon River in Allerton Park forming local anabranching, March 2005. (b) Same loop in February 2023. Google Earth Imagery. (c) Secondary channels on the floodplain of the Upper Sangamon River (USR) 22 km upstream from Allerton Park. (d) Wedge of sand in secondary channel in lee of wood jam, Allerton Park. (e) Picture of secondary channel SC1 depicting exposed tree roots on the bank. (f) Picture from SC5 depicting exposed roots on the bed. Trowel for scale. Inset in panel (a) shows the locations of (a), (b), (d), (e), and (f) within Allerton Park, and (c) within the USR.

convey flow at stages well below bankfull and create multithread river planforms (Rhoads, 2020). The persistence of multiple anabranching channels is evident on an elongated meander bend in the middle of the Allerton-Park study reach (Figures 13a and 13b). A chute-cutoff channel has existed on this loop for at least the past 25 years, yet water continues to flow around the bend and through the chute-cutoff channel, producing an anabranching planform. Several other anabranching reaches have been identified along the Sangamon River within several kilometers upstream and downstream of Allerton Park (Shukla & Rhoads, 2023). At least one of these anabranching reaches has existed in virtually the same planform configuration since the early 1800s, when it was documented on General Land Office survey maps. Other anabranching reaches appear to be stable over periods of several decades based on the inspection of historical aerial imagery. In close proximity to existing

anabranching reaches, lidar highlights an abundance of secondary channels on the floodplain, suggesting that these features may, in at least some instances, evolve into anabranches (Figure 13c).

5.5. Implications for Understanding Wood Jams Along Lowland River Floodplains

The higher density of wood jams within CSCs compared to DSCs may reflect more sustained transport of material through CSCs compared to DSCs. Wood delivered to CSCs from the main channel can potentially move throughout the entire length of these channels and become trapped locally behind obstacles, including live trees bordering or growing within these channels. By contrast, the diminishing size of DSCs may impede the transport of large wood along the entire length of these channels. In both types of secondary channels, the majority of wood jams are channel spanning and clustered along narrower or curved sections of the secondary channels where the movement of wood is impeded by changes in channel size or alignment (Cadol et al., 2009). The source of wood within secondary channels remains unknown. Some may be delivered to these channels by flow from the main channel, but other material likely originates from downed wood on the floodplain or within the secondary channels. Although the present study did not measure large wood abundance in other floodplain features, including the raised floodplain surface, field observations suggest that floodplain secondary channels may contain the highest density of active large wood jams on the floodplain; much of the large wood on the floodplain consists of fallen trees and branches. The greater abundance of large wood jams in the main channel of the Sangamon River compared to floodplain secondary channels is consistent with findings on wood abundance for the Congaree and Ogeechee Rivers as well as a mountainous stream system in the Chilean Andes (Benke & Wallace, 1990; Comiti et al., 2006; Wohl et al., 2011). Collectively, these results indicate that the densest storage of large wood occurs within the main channel of river systems.

5.6. Implications for Floodplain Restoration and Maintenance of Secondary Channels

The persistence of floodplain secondary channels on the Sangamon River floodplain over several years and perhaps much longer suggests that a hydrologic regime that inundates the floodplain regularly (8% of the days per year) is sufficient to maintain these channels. This result can help guide restoration efforts aimed at maintaining secondary channels on floodplains, particularly intentionally excavated channels, which in some cases have been found to be unstable and filled with sediment (Campana et al., 2014; Kristensen et al., 2014; Riquier et al., 2017; Roni et al., 2019; van Denderen et al., 2019). Recent work has demonstrated that secondary channels have a significant influence on the spatial composition of the floodplain forest community at Allerton Park and therefore play an important role in structuring the floodplain riparian ecosystem (Shukla et al., 2024). Future restoration projects that aim to improve the ecological potential of river systems through floodplain reconnection involving excavation of secondary channels should consider whether or not the prevailing hydrologic regime is suitable for the maintenance of secondary channels.

6. Conclusions

The results of this study advance our knowledge of secondary channels that develop on the floodplains of lowland meandering river systems with muddy floodplains. Secondary channels exhibit considerable spatial variability in their cross-sectional form and are distinct from both the main river channel and the floodplain surface in terms of the channel dimensions, sediment composition, and distribution of large wood jams. Secondary channels, which originate at low areas along the banks of the main channel and extend into the floodplain, are generally much smaller than the main channel; widths and depths of these channels are about one-third of the values for the main channel. The bankfull area (product of bankfull width and depth) of these channels varies spatially and this variability is associated with the orientation and degree of connectivity of secondary channels in relation to the main river channel. Discontinuous secondary channels tend to be oriented perpendicular to the direction of the main channel, and exhibit decreasing bankfull areas toward their distal ends. Continuous secondary channels may or may not decrease in size over distance. Bank elevations of all secondary channels exhibit considerable spatial variability so that connectivity between the secondary channels and the adjacent floodplain surface occurs over a range of water surface elevations, similar to the inundation dynamics for the main channel (Czuba et al., 2019; Lindroth et al., 2020).

The occurrence of zones of scour close to the proximal ends of several secondary channels suggests that hydraulic action is most effective at producing erosion where outflow from the main channel enters these channels. The

beds of secondary channels are generally more fine-grained than the bed of the main channel, consisting mainly of mud (76%) and fine sand (24%), but are slightly coarser than the surface of the adjacent floodplain. The texture of bank material in secondary channels is similar to the texture of floodplain-surface sediment and to bank material in the main channel. Bed material in secondary channels is somewhat coarser than bank material in these channels and in the main channel but much finer than bed material in the main channel. Together, these textural relations indicate that secondary channels are carved into floodplain sediment and do not convey the full size range of bed material in the main channel onto the floodplain. When activated, these channels primarily appear to be conduits for wash load and fine suspended load from the main channel. Secondary channels contain numerous wood jams and the density of jams is greater in CSCs than in DSCs; however, the density of wood in these channels is not as high as the density of wood in the main river channel.

Although flow occurs in secondary channels at stages below bankfull in the main channel, the beds of secondary channels only become nearly fully mobile when flows in the main channel exceed the bankfull stage. Thus, activation of bed-material transport within secondary channels appears to be stage-related and occurs only when substantial flow from the main river enters these channels. For the secondary channels examined in this study, bed-material mobilization is equaled or exceeded about 8% of the time (~30 days in a year). Flow can be sustained at a narrow range of stages below bankfull, but ponding also occurs locally within these secondary channels following floods (Shukla et al., 2024). At high stages, these channels not only are conduits for distributing water from the main river onto the floodplain but also potential sources of material that can be entrained from the secondary channel beds and redistributed to other parts of the floodplain.

Although field observations indicate that the secondary channels examined in this study persist over timescales of at least several years, their evolutionary trajectory remains unclear. The bed-material mobility analysis and existence of zones of scour suggest that erosion can occur within these channels, but the texture of bed material (mud and fine sand) is indicative of deposition of fine-grained suspended sediment. Further research is needed to determine whether the sediment balance of these channels is characterized by net erosion, net deposition, or a balance between erosion and deposition. Process-based field investigations of secondary channels are needed to examine flow, sediment transport, and patterns of erosion and deposition. Such investigations can help to determine whether secondary channels contribute to the process of anabranching along meandering rivers or whether these channels represent distinct stable features that differ from anabranches. Assessment of the long-term stability of secondary channels and the factors promoting stability will inform management efforts aimed at enhancing or re-establishing connections between main channels and floodplains.

Data Availability Statement

The lidar data used for setting up the HEC-RAS2D model in the study and extracting secondary channel bankfull geometry are available at https://clearinghouse.isgs.illinois.edu/data/elevation/illinois-height-modernization-ilhmp. The jupyter notebook for extracting bankfull dimensions is available as Shukla (2024).

Acknowledgments
Financial support was provided by the U.S. National Science Foundation Grant EAR-2012850 for the project Network Cluster CINET: Critical Interface Network in Intensively Managed Landscapes. The manuscript benefited from comments by three anonymous reviewers and the editor. We thank Molly Cain for providing instrumentation for the measurement of surface water levels.

References

Abbe, T. B., & Montgomery, D. R. (2003). Patterns and processes of wood debris accumulation in the Queets river basin, Washington. *Geomorphology*, *51*(1), 81–107. https://doi.org/10.1016/S0169-555X(02)00326-4

Anders, A. M., Bettis, E. A. I., Grimley, D. A., Stumpf, A. J., & Kumar, P. (2018). Impacts of Quaternary history on critical zone structure and processes: Examples and a conceptual model from the intensively managed landscapes critical zone observatory. *Frontiers in Earth Science*, *6*. https://doi.org/10.3389/feart.2018.00024

Baptist, M. J., Penning, W. E., Duel, H., Smits, A. J. M., Geerling, G. W., Van der Lee, G. E. M., & Van Alphen, J. S. L. (2004). Assessment of the effects of cyclic floodplain rejuvenation on flood levels and biodiversity along the Rhine River. *River Research and Applications*, *20*(3), 285–297. https://doi.org/10.1002/rra.778

Benke, A. C., Chaubey, I., Ward, G. M., & Dunn, E. L. (2000). Flood pulse dynamics of an unregulated river floodplain in the southeastern U.S. coastal plain. *Ecology*, *81*(10), 2730–2741. https://doi.org/10.1890/0012-9658(2000)081[2730:FPDOAU]2.0.CO;2

Benke, A. C., & Wallace, J. B. (1990). Wood dynamics in coastal plain blackwater streams. *Canadian Journal of Fisheries and Aquatic Sciences*, *47*(1), 92–99. https://doi.org/10.1139/f90-009

Brunner, G. W., Piper, S. S., Jensen, M. R., & Chacon, B. (2015). Combined 1D and 2D hydraulic modeling within HEC-RAS. In *World Environmental and Water Resources Congress 2015* (pp. 1432–1443). https://doi.org/10.1061/9780784479162.141

Buffington, J. M., Lisle, T. E., Woodsmith, R. D., & Hilton, S. (2002). Controls on the size and occurrence of pools in coarse-grained forest rivers. *River Research and Applications*, *18*(6), 507–531. https://doi.org/10.1002/rra.693

Buijse, A. D., Coops, H., Staras, M., Jans, L. H., Van Geest, G. J., Grift, R. E., et al. (2002). Restoration strategies for river floodplains along large lowland rivers in Europe. *Freshwater Biology*, *47*(4), 889–907. https://doi.org/10.1046/j.1365-2427.2002.00915.x

Cadol, D., Wohl, E., Goode, J. R., & Jaeger, K. L. (2009). Wood distribution in neotropical forested headwater streams of La Selva, Costa Rica. *Earth Surface Processes and Landforms*, *34*(9), 1198–1215. https://doi.org/10.1002/esp.1800

Cain, M. R. (2022). Linking dynamic connectivity and hydrologic response. [Ph.D., Indiana University]. In *ProQuest dissertations and theses (2705710638)*. Dissertations & Theses @ CIC Institutions; ProQuest Dissertations & Theses Global. Retrieved from https://www.proquest.com/dissertations-theses/linking-dynamic-connectivity-hydrologic-response/docview/2705710638/se-2?accountid=14553

Campana, D., Marchese, E., Theule, J. I., & Comiti, F. (2014). Channel degradation and restoration of an Alpine river and related morphological changes. *Geomorphology*, *221*, 230–241. https://doi.org/10.1016/j.geomorph.2014.06.016

Cashman, M. J., Harvey, G. L., & Wharton, G. (2021). Structural complexity influences the ecosystem engineering effects of in-stream large wood. *Earth Surface Processes and Landforms*, *46*(10), 2079–2091. https://doi.org/10.1002/esp.5145

Castillo, C. R., Güneralp, İ., Hales, B., & Güneralp, B. (2020). Scale-free structure of surface-water connectivity within a lowland river-floodplain landscape. *Geophysical Research Letters*, *47*(16), e2020GL088378. https://doi.org/10.1029/2020GL088378

Chen, D., Zheng, J., Zhang, C., Guan, D., Li, Y., & Wang, Y. (2021). Critical shear stress for erosion of sand-mud mixtures and pure mud. *Frontiers in Marine Science*, *8*. https://doi.org/10.3389/fmars.2021.713039

Chowdhury, M. K., Konsoer, K. M., & Hiatt, M. (2022). Effect of lateral outflow on three-dimensional flow structure in a river delta. *Water Resources Research*, *58*(10), e2021WR031346. https://doi.org/10.1029/2021WR031346

Comiti, F., Andreoli, A., Lenzi, M. A., & Mao, L. (2006). Spatial density and characteristics of woody debris in five mountain rivers of the Dolomites (Italian Alps). *Geomorphology*, *78*(1), 44–63. https://doi.org/10.1016/j.geomorph.2006.01.021

Constantine, J. A., McLean, S. R., & Dunne, T. (2010). A mechanism of chute cutoff along large meandering rivers with uniform floodplain topography. *GSA Bulletin*, *122*(5–6), 855–869. https://doi.org/10.1130/B26560.1

Curry, B. B., Grimley, D. A., & McKay, E. D. (2011). Chapter 36—Quaternary glaciations in Illinois. In J. Ehlers, P. L. Gibbard, & P. D. Hughes (Eds.), *Developments in quaternary sciences* (Vol. 15, pp. 467–487). Elsevier. https://doi.org/10.1016/B978-0-444-53447-7.00036-2

Czuba, J. A., David, S. R., Edmonds, D. A., & Ward, A. S. (2019). Dynamics of surface-water connectivity in a low-gradient meandering river floodplain. *Water Resources Research*, *55*(3), 1849–1870. https://doi.org/10.1029/2018WR023527

David, S. R., Czuba, J. A., & Edmonds, D. A. (2018). Channelization of meandering river floodplains by headcutting. *Geology*, *47*(1), 15–18. https://doi.org/10.1130/G45529.1

David, S. R., Edmonds, D. A., & Letsinger, S. L. (2017). Controls on the occurrence and prevalence of floodplain channels in meandering rivers. *Earth Surface Processes and Landforms*, *42*(3), 460–472. https://doi.org/10.1002/esp.4002

Day, G., Dietrich, W. E., Rowland, J. C., & Marshall, A. (2008). The depositional web on the floodplain of the Fly River, Papua New Guinea. *Journal of Geophysical Research*, *113*(F1). https://doi.org/10.1029/2006JF000622

Dixon, S. J. (2016). A dimensionless statistical analysis of logjam form and process. *Ecohydrology*, *9*(6), 1117–1129. https://doi.org/10.1002/eco.1710

Dunn, I. S. (1959). Tractive resistance of cohesive channels. *Journal of the Soil Mechanics and Foundations Division*, *85*(3), 1–24. https://doi.org/10.1061/JSFEAQ.0000195

Fagan, S. D., & Nanson, G. C. (2004). The morphology and formation of floodplain-surface channels, Cooper Creek, Australia. *Geomorphology*, *60*(1), 107–126. https://doi.org/10.1016/j.geomorph.2003.07.009

Fehrenbacher, J. B., Olson, K. R., & Jansen, I. J. (1986). Loess thickness in Illinois. *Soil Science*, *141*(6), 423–431. https://doi.org/10.1097/00010694-198606000-00004

Funk, A., Baldan, D., Bondar-Kunze, E., Brizuela, S. R., Kowal, J., & Hein, T. (2023). Connectivity as a driver of river-floodplain functioning: A dynamic, graph theoretic approach. *Ecological Indicators*, *154*, 110877. https://doi.org/10.1016/j.ecolind.2023.110877

Galia, T., Kuglerová, L., & Škarpich, V. (2024). Floodplain and in-channel large wood storage in the fluvial corridor of an actively meandering river. *Forest Ecology and Management*, *557*, 121770. https://doi.org/10.1016/j.foreco.2024.121770

Garcia, M. (2008). *Sedimentation engineering: Processes, measurements, modeling, and practice*. American Society of Civil Engineers (ASCE).

Graf, W. L. (2006). Downstream hydrologic and geomorphic effects of large dams on American rivers. *Geomorphology*, *79*(3), 336–360. https://doi.org/10.1016/j.geomorph.2006.06.022

Grimley, D. A., Anders, A. M., Bettis, E. A., Bates, B. L., Wang, J. J., Butler, S. K., & Huot, S. (2017). Using magnetic fly ash to identify post-settlement alluvium and its record of atmospheric pollution, central USA. *Anthropocene*, *17*, 84–98. https://doi.org/10.1016/j.ancene.2017.02.001

Grimley, D. A., Anders, A. M., & Stumpf, A. J. (2016). Quaternary geology of the Upper Sangamon River Basin: Glacial, postglacial, and postsettlement history. In *Celebrating 50 Years of geoscience in the mid-continent: Guidebook for the 50th Annual Meeting of the Geological Society of America – North-Central section, April 18–19, 2016. Illinois state geological survey, guidebook* (Vol. 43, pp. 55–96). University of Illinois Board of Trustees.

Hardy, R. J., Bates, P. D., & Anderson, M. G. (2000). Modelling suspended sediment deposition on a fluvial floodplain using a two-dimensional dynamic finite element model. *Journal of Hydrology*, *229*(3), 202–218. https://doi.org/10.1016/S0022-1694(00)00159-1

He, C., Taylor, J. N., Rochfort, Q., & Nguyen, D. (2021). A new portable in situ flume for measuring critical shear stress on river beds. *International Journal of Sediment Research*, *36*(2), 235–242. https://doi.org/10.1016/j.ijsrc.2020.08.004

He, Q., & Walling, D. E. (1998). An investigation of the spatial variability of the grain size composition of floodplain sediments. *Hydrological Processes*, *12*(7), 1079–1094. https://doi.org/10.1002/(SICI)1099-1085(19980615)12:7<1079::AID-HYP642>3.0.CO;2-E

Herrero, A., Bateman, A., & Medina, V. (2015). Water flow and sediment transport in a 90° channel diversion: An experimental study. *Journal of Hydraulic Research*, *53*(2), 253–263. https://doi.org/10.1080/00221686.2014.989457

Hir, P. L., Cann, P., Waeles, B., Jestin, H., & Bassoullet, P. (2008). Chapter 11 Erodibility of natural sediments: Experiments on sand/mud mixtures from laboratory and field erosion tests. In T. Kusuda, H. Yamanishi, J. Spearman, & J. Z. Gailani (Eds.), *Proceedings in marine science* (Vol. 9, pp. 137–153). Elsevier. https://doi.org/10.1016/S1568-2692(08)80013-7

Hoffmans, G., & van Rijn, L. (2018). Hydraulic approach for predicting piping in dikes. *Journal of Hydraulic Research*, *56*(2), 268–281. https://doi.org/10.1080/00221686.2017.1315747

Iskin, E. P., & Wohl, E. (2023). Beyond the case study: Characterizing natural floodplain heterogeneity in the United States. *Water Resources Research*, *59*(8), e2023WR035162. https://doi.org/10.1029/2023WR035162

Jacobs, W., Le Hir, P., Van Kesteren, W., & Cann, P. (2011). Erosion threshold of sand–mud mixtures. *Continental Shelf Research*, *31*(10, Supplement), S14–S25. https://doi.org/10.1016/j.csr.2010.05.012

Jones, J. L. (2006). Side channel mapping and fish habitat suitability analysis using lidar topography and orthophotography. *Photogrammetric Engineering*.

Keefer, L., & Bauer, E. (2011). Upper Sangamon River Watershed monitoring data for the USEPA Targeted Watershed Study: 2005-2008. ISWS Contract Report CR-2011-03. https://hdl.handle.net/2142/39554

Kempton, J. P., Johnson, W. H., Heigold, P. C., & Cartwright, K. (1991). Mahomet Bedrock Valley in east-central Illinois; Topography, glacial drift stratigraphy, and hydrogeology. In W. N. Melhorn & J. P. Kempton (Eds.), *Geology and hydrogeology of the Teays-Mahomet Bedrock Valley System* (Vol. 258, pp. 0–124). Geological Society of America. https://doi.org/10.1130/SPE258-p91

Kleinhans, M. G., de Haas, T., Lavooi, E., & Makaske, B. (2012). Evaluating competing hypotheses for the origin and dynamics of river anastomosis. *Earth Surface Processes and Landforms*, *37*(12), 1337–1351. https://doi.org/10.1002/esp.3282

Kothyari, U. C., & Jain, R. K. (2008). Influence of cohesion on the incipient motion condition of sediment mixtures. *Water Resources Research*, *44*(4). https://doi.org/10.1029/2007WR006326

Kristensen, E. A., Kronvang, B., Wiberg-Larsen, P., Thodsen, H., Nielsen, C., Amor, E., et al. (2014). 10 years after the largest river restoration project in Northern Europe: Hydromorphological changes on multiple scales in River Skjern. *Ecological Engineering*, *66*, 141–149. https://doi.org/10.1016/j.ecoleng.2013.10.001

Latterell, J. J., Scott Bechtold, J., O'keefe, T. C., Van Pelt, R., & Naiman, R. J. (2006). Dynamic patch mosaics and channel movement in an unconfined river valley of the Olympic Mountains. *Freshwater Biology*, *51*(3), 523–544. https://doi.org/10.1111/j.1365-2427.2006.01513.x

Lindroth, E. M., Rhoads, B. L., Castillo, C. R., Czuba, J. A., Güneralp, İ., & Edmonds, D. (2020). Spatial variability in bankfull stage and bank elevations of lowland meandering rivers: Relation to rating curves and channel planform characteristics. *Water Resources Research*, *56*(8), e2020WR027477. https://doi.org/10.1029/2020wr027477

Lininger, K. B., Scamardo, J. E., & Guiney, M. R. (2021). Floodplain large wood and organic matter jam formation after a large flood: Investigating the influence of floodplain forest stand characteristics and river corridor morphology. *Journal of Geophysical Research: Earth Surface*, *126*(6), e2020JF006011. https://doi.org/10.1029/2020JF006011

Livers, B., Lininger, K. B., Kramer, N., & Sendrowski, A. (2020). Porosity problems: Comparing and reviewing methods for estimating porosity and volume of wood jams in the field. *Earth Surface Processes and Landforms*, *45*(13), 3336–3353. https://doi.org/10.1002/esp.4969

Makaske, B., Lavooi, E., de Haas, T., Kleinhans, M. G., & Smith, D. G. (2017). Upstream control of river anastomosis by sediment overloading, upper Columbia River, British Columbia, Canada. *Sedimentology*, *64*(6), 1488–1510. https://doi.org/10.1111/sed.12361

Makaske, B., Smith, D. G., & Berendsen, H. J. A. (2002). Avulsions, channel evolution and floodplain sedimentation rates of the anastomosing upper Columbia River, British Columbia, Canada. *Sedimentology*, *49*(5), 1049–1071. https://doi.org/10.1046/j.1365-3091.2002.00489.x

Marriott, S. (1992). Textural analysis and modelling of a flood deposit: River severn, U.K. *Earth Surface Processes and Landforms*, *17*(7), 687–697. https://doi.org/10.1002/esp.3290170705

Mattingly, R. L., Herricks, E. E., & Johnston, D. M. (1993). Channelization and levee construction in Illinois: Review and implications for management. *Environmental Management*, *17*(6), 781–795. https://doi.org/10.1007/BF02393899

May, C. L., & Gresswell, R. E. (2003). Processes and rates of sediment and wood accumulation in headwater streams of the Oregon Coast Range, USA. *Earth Surface Processes and Landforms*, *28*(4), 409–424. https://doi.org/10.1002/esp.450

Mertes, L. A. K., Dunne, T., & Martinelli, L. A. (1996). Channel-floodplain geomorphology along the Solimões-Amazon River, Brazil. *GSA Bulletin*, *108*(9), 1089–1107. https://doi.org/10.1130/0016-7606(1996)108<1089:CFGATS>2.3.CO;2

Moody, J. A., Pizzuto, J. E., & Meade, R. H. (1999). Ontogeny of a flood plain. *GSA Bulletin*, *111*(2), 291–303. https://doi.org/10.1130/0016-7606(1999)111<0291:OOAFP>2.3.CO;2

Nicholas, A. P., & McLelland, S. J. (2004). Computational fluid dynamics modelling of three-dimensional processes on natural river floodplains. *Journal of Hydraulic Research*, *42*(2), 131–143. https://doi.org/10.1080/00221686.2004.9728377

Nicholas, A. P., & Walling, D. E. (1997). Modelling flood hydraulics and overbank deposition on river floodplains. *Earth Surface Processes and Landforms*, *22*(1), 59–77. https://doi.org/10.1002/(SICI)1096-9837(199701)22:1<59::AID-ESP652>3.0.CO;2-R

Nienhuis, P. H., Buijse, A. D., Leuven, R. S. E. W., Smits, A. J. M., de Nooij, R. J. W., & Samborska, E. M. (2002). Ecological rehabilitation of the lowland basin of the river Rhine (NW Europe). *Hydrobiologia*, *478*(1), 53–72. https://doi.org/10.1023/A:1021070428566

Ochs, C. A., & Shields Jr., F. D. (2019). Fluxes of nutrients and primary production between the main channel and floodplain backwaters of the Lower Mississippi River—Development of a simulation model. *River Research and Applications*, *35*(7), 979–988. https://doi.org/10.1002/rra.3482

Panagiotopoulos, I., Voulgaris, G., & Collins, M. B. (1997). The influence of clay on the threshold of movement of fine sandy beds. *Coastal Engineering*, *32*(1), 19–43. https://doi.org/10.1016/S0378-3839(97)00013-6

Perera, C., Smith, J., Wu, W., Perkey, D., & Priestas, A. (2020). Erosion rate of sand and mud mixtures. *International Journal of Sediment Research*, *35*(6), 563–575. https://doi.org/10.1016/j.ijsrc.2020.06.004

Piégay, H., Hupp, C. R., Citterio, A., Dufour, S., Moulin, B., & Walling, D. E. (2008). Spatial and temporal variability in sedimentation rates associated with cutoff channel infill deposits: Ain River, France. *Water Resources Research*, *44*(5). https://doi.org/10.1029/2006WR005260

Rhoads, B. L. (2020). *River dynamics: Geomorphology to support management*. Cambridge University Press.

Rhoads, B. L., Anders, A. M., Banerjee, P., Grimley, D. A., Stumpf, A., & Blair, N. E. (2024). Sensitivity of a meandering lowland river to intensive landscape management: Lateral migration rates before and after watershed-scale agricultural development. *Anthropocene*, *45*, 100429. https://doi.org/10.1016/j.ancene.2024.100429

Rhoads, B. L., & Herricks, E. E. (1996). Naturalization of headwater streams in Illinois: Challenges and possibilities. In *River channel restoration: Guiding principles for sustainable projects* (pp. 331–367).

Rhoads, B. L., Lewis, Q. W., & Andresen, W. (2016). Historical changes in channel network extent and channel planform in an intensively managed landscape: Natural versus human-induced effects. *Geomorphology*, *252*, 17–31. https://doi.org/10.1016/j.geomorph.2015.04.021

Riquier, J., Piégay, H., Lamouroux, N., & Vaudor, L. (2017). Are restored side channels sustainable aquatic habitat features? Predicting the potential persistence of side channels as aquatic habitats based on their fine sedimentation dynamics. *Geomorphology*, *295*, 507–528. https://doi.org/10.1016/j.geomorph.2017.08.001

Riquier, J., Piégay, H., & Šulc Michalková, M. (2015). Hydromorphological conditions in eighteen restored floodplain channels of a large river: Linking patterns to processes. *Freshwater Biology*, *60*(6), 1085–1103. https://doi.org/10.1111/fwb.12411

Roni, P., Hall, J. E., Drenner, S. M., & Arterburn, D. (2019). Monitoring the effectiveness of floodplain habitat restoration: A review of methods and recommendations for future monitoring. *WIREs Water*, *6*(4), e1355. https://doi.org/10.1002/wat2.1355

Rowland, J. C., Dietrich, W. E., Day, G., & Parker, G. (2009). Formation and maintenance of single-thread tie channels entering floodplain lakes: Observations from three diverse river systems. *Journal of Geophysical Research*, *114*(F2). https://doi.org/10.1029/2008JF001073

Ruiz-Villanueva, V., Piégay, H., Gurnell, A. M., Marston, R. A., & Stoffel, M. (2016). Recent advances quantifying the large wood dynamics in river basins: New methods and remaining challenges. *Reviews of Geophysics*, *54*(3), 611–652. https://doi.org/10.1002/2015RG000514

Salas, C. R., & Rhoads, B. L. (2024). Spatial and temporal variations of suspended sediment concentrations from different floodplain environments. In *River flow 2022*. CRC Press.

Schäfer Rodrigues Silva, A., Noack, M., Schlabing, D., & Wieprecht, S. (2018). A data-driven fuzzy approach to simulate the critical shear stress of mixed cohesive/non-cohesive sediments. *Journal of Soils and Sediments*, *18*(10), 3070–3081. https://doi.org/10.1007/s11368-017-1860-8

Schropp, M. h. i., & Bakker, C. (1998). Secondary channels as a basis for the ecological rehabilitation of Dutch rivers. *Aquatic Conservation: Marine and Freshwater Ecosystems*, *8*(1), 53–59. https://doi.org/10.1002/(SICI)1099-0755(199801/02)8:1<53::AID-AQC260>3.0.CO;2-O

Sharif, A. R. (2003). Critical shear stress and erosion of cohesive soils. [Ph.D., State University of New York at Buffalo]. https://www.proquest.com/docview/305244640/abstract/87E2FC22F4D84CB1PQ/1

Shukla, T. (2024). Bankfull dimensions of river channels [Code]. https://doi.org/10.5281/zenodo.13763244

Shukla, T., Chelsy R, S., Ryan C, P., & Bruce, L. R. (2024). Critical linkages among floodplain hydrology, geomorphology, and ecology along a lowland meandering river, Illinois, USA. *Ecohydrology*, *17*(6), e2661. https://doi.org/10.1002/eco.2661

Shukla, T., & Rhoads, B. L. (2023). Meandering rivers that anabranch in the upper Midwest (USA): Prevalence, morphological characteristics, and power regimes. *Geomorphology*, *440*, 108854. https://doi.org/10.1016/j.geomorph.2023.108854

Simons, J. H. E. J., Bakker, C., Schropp, M. H. I., Jans, L. H., Kok, F. R., & Grift, R. E. (2001). Man-made secondary channels along the River Rhine (The Netherlands); results of post-project monitoring. *Regulated Rivers: Research & Management*, *17*(4–5), 473–491. https://doi.org/10.1002/rrr.661

Smerdon, E., & Beasley, R. P. (1959). The tractive force theory applied to stability of open channels in cohesive soils. Retrieved from https://www.semanticscholar.org/paper/The-tractive-force-theory-applied-to-stability-of-Smerdon-Beasley/07eb2752bc7758f2d81e94e94ac29fe5cf7517dd

Sumaiya, S., Czuba, J. A., Schubert, J. T., David, S. R., Johnston, G. H., & Edmonds, D. A. (2021). Sediment transport potential in a hydraulically connected river and floodplain-channel system. *Water Resources Research*, *57*(5), e2020WR028852. https://doi.org/10.1029/2020WR028852

Sumaiya, S., Schubert, J. T., Czuba, J. A., & Pizzuto, J. E. (2024). Incorporating flowpaths as an explicit measure of river-floodplain connectivity to improve estimates of floodplain sediment deposition. *Geomorphica*, *1*(1). Article 1. https://doi.org/10.59236/geomorphica.v1i1.25

Thayer, J. B., & Ashmore, P. (2016). Floodplain morphology, sedimentology, and development processes of a partially alluvial channel. *Geomorphology*, *269*, 160–174. https://doi.org/10.1016/j.geomorph.2016.06.040

Thompson, D. M. (2003). A geomorphic explanation for a meander cutoff following channel relocation of a coarse-bedded river. *Environmental Management*, *31*(3), 0385–0400. https://doi.org/10.1007/s00267-002-2842-0

Torfs, H. (1995). Proefschrift voorgedragen tot het behalen van het doctoraat in de toegepaste wetenschappen.

Trigg, M. A., Bates, P. D., Wilson, M. D., Schumann, G., & Baugh, C. (2012). Floodplain channel morphology and networks of the middle Amazon River. *Water Resources Research*, *48*(10). https://doi.org/10.1029/2012WR011888

Tull, N., Moodie, A. J., & Passalacqua, P. (2024). River-floodplain connectivity and residence times controlled by topographic bluffs along a backwater transition. *Frontiers in Water*, *5*. https://doi.org/10.3389/frwa.2023.1306481

Urban, M. A., & Rhoads, B. L. (2003). Catastrophic human-induced change in stream-channel planform and geometry in an agricultural watershed, Illinois, USA. *Annals of the Association of American Geographers*, *93*(4), 783–796. https://doi.org/10.1111/j.1467-8306.2003.09304001.x

van Denderen, R. P., Schielen, R. M. J., Westerhof, S. G., Quartel, S., & Hulscher, S. J. M. H. (2019). Explaining artificial side channel dynamics using data analysis and model calculations. *Geomorphology*, *327*, 93–110. https://doi.org/10.1016/j.geomorph.2018.10.016

van der Steeg, S., Torres, R., Viparelli, E., Xu, H., Elias, E., & Sullivan, J. C. (2023). Floodplain surface-water circulation dynamics: Congaree River, South Carolina, USA. *Water Resources Research*, *59*(1), e2022WR032982. https://doi.org/10.1029/2022WR032982

van Dijk, W. M., Schuurman, F., van de Lageweg, W. I., & Kleinhans, M. G. (2014). Bifurcation instability and chute cutoff development in meandering gravel-bed rivers. *Geomorphology*, *213*, 277–291. https://doi.org/10.1016/j.geomorph.2014.01.018

van Rijn, L. (2020). Erodibility of mud–sand bed mixtures. *Journal of Hydraulic Engineering*, *146*(1), 04019050. https://doi.org/10.1061/(ASCE)HY.1943-7900.0001677

Ventres-Pake, R., Nahorniak, M., Kramer, N., O'Neal, J., & Abbe, T. (2020). Integrating large wood jams into hydraulic models: Evaluating a porous plate modeling method. *Journal of the American Water Resources Association*, *56*(2), 333–347. https://doi.org/10.1111/1752-1688.12818

Viero, D. P., Dubon, S. L., & Lanzoni, S. (2018). Chute cutoffs in meandering rivers: Formative mechanisms and hydrodynamic forcing. In *Fluvial meanders and their sedimentary products in the rock record* (pp. 201–229). John Wiley & Sons, Ltd. https://doi.org/10.1002/9781119424437.ch8

Wilcock, P. R., & Kenworthy, S. T. (2002). A two-fraction model for the transport of sand/gravel mixtures. *Water Resources Research*, *38*(10), 12-1–12-12. https://doi.org/10.1029/2001WR000684

Wohl, E. (2013). Floodplains and wood. *Earth-Science Reviews*, *123*, 194–212. https://doi.org/10.1016/j.earscirev.2013.04.009

Wohl, E., Cenderelli, D. A., Dwire, K. A., Ryan-Burkett, S. E., Young, M. K., & Fausch, K. D. (2010). Large in-stream wood studies: A call for common metrics. *Earth Surface Processes and Landforms*, *35*(5), 618–625. https://doi.org/10.1002/esp.1966

Wohl, E., Polvi, L. E., & Cadol, D. (2011). Wood distribution along streams draining old-growth floodplain forests in Congaree National Park, South Carolina, USA. *Geomorphology*, *126*(1), 108–120. https://doi.org/10.1016/j.geomorph.2010.10.035

Xu, H., Torres, R., van der Steeg, S., & Viparelli, E. (2021). Geomorphology of the Congaree river floodplain: Implications for the inundation continuum. *Water Resources Research*, *57*(12), e2020WR029456. https://doi.org/10.1029/2020WR029456

Xu, H., van der Steeg, S., Sullivan, J., Shelley, D., Cely, J. E., Viparelli, E., et al. (2020). Intermittent channel systems of a low-relief, low-gradient floodplain: Comparison of automatic extraction methods. *Water Resources Research*, *56*(9), e2020WR027603. https://doi.org/10.1029/2020WR027603

Zhang, M., & Yu, G. (2017). Critical conditions of incipient motion of cohesive sediments. *Water Resources Research*, *53*(9), 7798–7815. https://doi.org/10.1002/2017WR021066